(1)

NUMERIC MODEL OF A CO_2 LASER AMPLIFIER

THESIS

Frank Patrick Gallagher
Captain, USAF

AFIT/GSO/ENP/ENS/89D-2

DEPARTMENT OF THE AIR FORCE
AIR UNIVERSITY
AIR FORCE INSTITUTE OF TECHNOLOGY

Wright-Patterson Air Force Base, Ohio

AFIT/GSO/ENP/ENS/89D-2

NUMERIC MODEL OF A CO_2 LASER AMPLIFIER

THESIS

Frank Patrick Gallagher
Captain, USAF

AFIT/GSO/ENP/ENS/89D-2

Approved for public release; distribution unlimited.

AFIT/GSO/ENP/ENS/89D-2

NUMERIC MODEL OF A CO_2 LASER AMPLIFIER

THESIS

Presented to the Faculty of the School of Engineering

of the Air Force Institute of Technology

Air University

In Partial Fulfillment of the

Requirements for the Degree of

Master of Science in Space Operations

Frank Patrick Gallagher, B.S.

Captain, USAF

December, 1989

Preface

The goal of this thesis was to develop and validate a CO_2 laser amplifier model that could be used both as a design aid and an instructional tool. As a design aid, the model's consideration of amplifier physics had to be thorough enough to provide accurate data while allowing the user to vary many design parameters. As an intructional tool, the model's user interface had to be simple and straightforward so the student would spend less time learning how to use another computer program and more time learning laser amplifier concepts.

In the chapters that follow, I describe the development and validation of this model as well as the limitations on its performance. In my writing, I assumed that readers of this thesis will have been introduced to CO_2 laser physics. As preliminary reading, I recommend the papers by Gilbert (7) and Patel (16).

I would like to thank my advisors, Dr. D. H. Stone, Dr. T. S. Kelso, and Dr. D. E. Beller, for their time and effort in helping me complete this project.

Frank Patrick Gallagher

Table of Contents

List of Figures

List of Tables

Abstract

A CO_2 laser amplifier simulation model is developed for use on IBM-compatible personal computers. First, a general laser amplifier is modeled by dividing an amplifier into separate cells to model both the temporal and spatial dependence of the amplifier's gain. The resulting amplification is validated by comparison with a closed-form solution. Second, losses due to amplified spontaneous emissions (ASE) are investigated and included in the model. Equations for ASE losses consider both the solid angle of the emissions and the reflectivity of the cavity windows. Other reflections are ignored. Third, an existing numerical model of CO_2 gas kinetics is incorporated. In this kinetics model, temperature-dependent terms are fixed according to initial conditions, and the rotational levels of the upper CO_2 vibrational state are assumed to be in equilibrium.

The user-friendly model allows designers and students to investigate the amplification of either square input pulses or pulses generated with a laser oscilltor while varying several input parameters. Among the variable parameters are length, diameter, gas mix, temperature, pressure, window reflectivity, and pump efficiency.

NUMERIC MODEL OF A CO_2 LASER AMPLIFIER

I. Background

As a program, this amplifier model is complete in itself, but it is designed to supplement an existing oscillator model. This chapter will begin with a brief description of the oscillator model. Next, the need for an amplifier model is presented. Finally, the scope of this project is outlined.

1.1 Original Model

Recently, a computer simulation model of an atmospheric-pressure, carbon dioxide (CO_2) laser oscillator was developed by Major David Stone. The model is programmed in *Quick BASIC* for use on IBM-compatible personal computers. It has been used in introductory laser physics courses to give students an appreciation for the design of laser radar transmitters. Stone's model uses a numeric approach similar to the one outlined by Gilbert (7). This model traces the time-varying populations of the 001 and 100 vibrational levels of CO_2 and the metastable (v=1) level of nitrogen under the influence of an idealized pump, gas kinetics, and a growing photon flux. The kinetic relationships between these gases and the development of a population inversion are described with coupled differential equations and experimentally-determined rate constants. These equations are solved iteratively using a fourth-order Runge-Kutta integration method.

1.2 Added Parameters

To make the model more precise, several changes to the original model have been made. First, Stone uses Witteman's equations for the rate constants used in the differential equations (25). These equations describe the dependence of the rate constants on pressure and the relative percentages of the species in the gas mix. Second, work by Melançon has been included to model the temperature dependence of the rate constants (13). Third,

Stone has added an option that will allow the "ideal" pump to be modeled as a half-sine-wave rather than a square wave. With all these changes, the model currently allows the following input parameters: pressure; relative percentages of CO_2, nitrogen, helium, hydrogen, and water vapor; temperature; and pump pulse shape, duration, and efficiency.

Additional parameters relate directly to aspects of laser radar design. Isotopes of CO_2 vary in their ability to transmit through the atmosphere and have different pulse-forming characteristics. To help analyze any tradeoffs that may exist, Stone has incorporated the Einstein coefficients of spontaneous emission for carbon-12 (^{12}C) and carbon-13 (^{13}C) as determined by Glazenkov (8:535-536). The last parameter is a decision on whether or not to use a Q-switch to create a sharper, more intense pulse. The optimization of Q-switching is part of laser radar design because the tracking of fast distant objects requires short intense pulses to provide high-resolution range measurements (6:2).

1.3 Amplifier Significance

Stone's model does not treat every aspect of laser radar design. Two missing considerations deal with power limitations. They are frequency stability and mirror damage. A laser radar system determines the velocity of a target by measuring the change in frequency of the return signal (Doppler analysis). Accurate velocity measurement requires high-frequency stability. This requirement, however, conflicts with the high power required for long-range tracking. According to Reilly:

> Very often the laser radar must have power levels in excess of a few hundred watts (CW or repetitive pulse average power). The use of a simple (CO_2) laser can produce satisfactory frequency stability up to power levels of a few tens of watts. Beyond these power levels the stability of the laser resonator often becomes a problem. ... the price of frequency stability, unfortunately, is low power (18:60).

Power is also limited by the material used for cavity mirrors. Most available materials have some absorption at the primary CO_2 laser wavelength, 10.6μm. Therefore, CO_2 lasers are notorious for inducing mirror damage (11:5077). For example, the damage thresholds for single crystalline molybdenum and single crystalline copper are 60 and 115 J/cm^2

respectively (23:415). Together, the requirements for high power, frequency stability and increased mirror life necessitate the use of laser amplifiers.

Several studies have confirmed master oscillator/power amplifier (MOPA) systems using CO_2 lasers to be the most effective laser radar transmitters (10, 18, 26, 9). In this system, the master oscillator generates a low-power, spectrally pure beam. This beam then propagates through a power amplifier where its energy increases, its pulsewidth narrows, and its frequency characteristics are preserved.

1.4 Purpose and Scope

To add another dimension to Stone's mod , it is the purpose of this thesis to develop and validate a model of a CO_2 laser radar amplifier. The key to modeling the pulse amplification process is determining the population inversion encountered by each slice of an oscillator's input pulse. Like the oscillator model, this model uses a fourth-order Runge-Kutta integration method to calculate the inversion at any time. However, the inversion within the amplifier is not spatially constant, so this model also calculates the inversion for each axial position within the amplifier.

Factors affecting this inversion included in the model are electrical pumping, collisional relaxation, stimulated emission, amplified spontaneous emission (ASE), and emissions reflected between the cavity windows. The portion of the input pulse that is reflected back into the amplifier will be considered a loss term and will not contribute to the output pulse. Emissions that are not axially directed, including wall reflections, are ignored. Because this model considers the amplification of only a single pulse, factors that determine pulse repetition frequency will not be addressed.

II. Model Development

This chapter contains theory applicable to modeling the processes of laser amplification and ASE. In general, the amplification process can be described by two nonlinear differential equations. These equations relate to the coupled relationship between the growing photon density and the deteriorating inversion. Because the modeled inversion is influenced by gas kinetics, these equations must be solved with numerical integrations rather than closed-form solutions. The interested reader is directed to the manuscript by Schulz-DuBois for a more rigorous treatment of these equations (20). During the following discussion, variables used in the model will be introduced to provide a clear transition from theory to modeling.

2.1 Amplifier Fundamentals

Consistent with basic laser theory, we are interested in the interaction between photons and a medium where a population inversion exists. Both the photon density and the population inversion vary as functions of time and position within the amplifier. In actual amplifiers, the population inversion and, consequently, the photon density have a three-dimensional position function. Measurements taken by McQuillan and Carswell have shown this function to depend on several parameters (12). Among the parameters listed are: gas composition, pressure, wall temperature, and tube diameter. A high-power amplifier model that incorporates all of these parameters on a two-dimensional level has been developed by Comly (3). Their model was created for the study of laser fusion and was not concerned with frequency stability, therefore it cannot be directly applied to the analysis of laser radar transmitters.

In our one-dimensional model we calculate only the longitudinal time variation of population inversion and photon density. In other words, we have assumed both variables to be constant for any cross section of the amplifier. By assuming cross-sectional invariance, we can also assume the diameter of the input beam is equal to the diameter of the amplifier. This assumption simplifies our population density calculations.

In the absence of a photon pulse, the population inversion across the entire amplifier is also uniform. However, once a pulse of photons enters the cavity, the spatial dependence of the population inversion cannot be ignored. The leading edge of the pulse experiences the original full inversion, but because it extracts energy as it propagates through the amplifier, the amount of energy stored in the inversion is reduced. This loss of energy results in a smaller population inversion.[1] Therefore, the remainder of the pulse will be amplified by a progressively smaller factor. Figure 2.1 illustrates the exponential growth

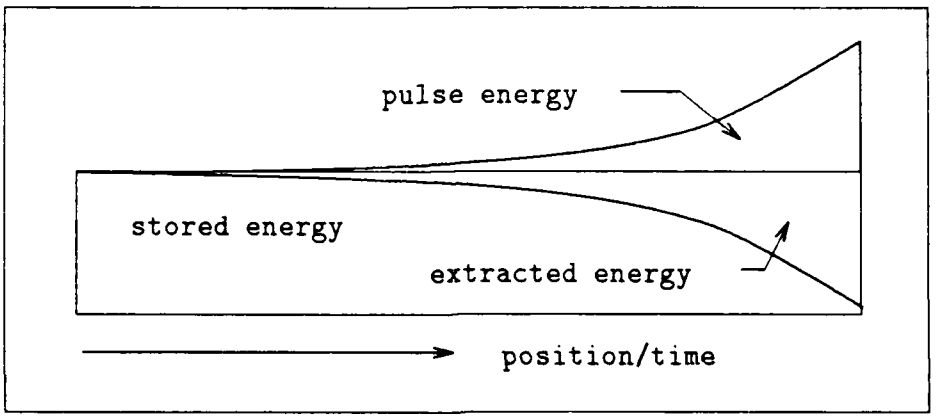

Figure 2.1. Pulse growth and energy extraction

of the leading edge and the resulting change in the energy stored for each position in the amplifier.

2.2 Amplifier Modeling

One approach to calculating the population inversion as a function of time and position is presented by Douglas-Hamilton *et al.* (4:76-77). As shown in Figure 2.2, they divide the amplifier into N cells, each having a length of L/N. By assuming the inversion across each cell is constant, the spatial dependence is removed and the calculation for the inversion is done as a function of time only. With increased values for N, the approxima-

[1] For every photon emitted by this stimulated emission process, the population of molecules in the upper energy state is reduced by one and the population of molecules in the lower energy state is increased by one—a net change of two.

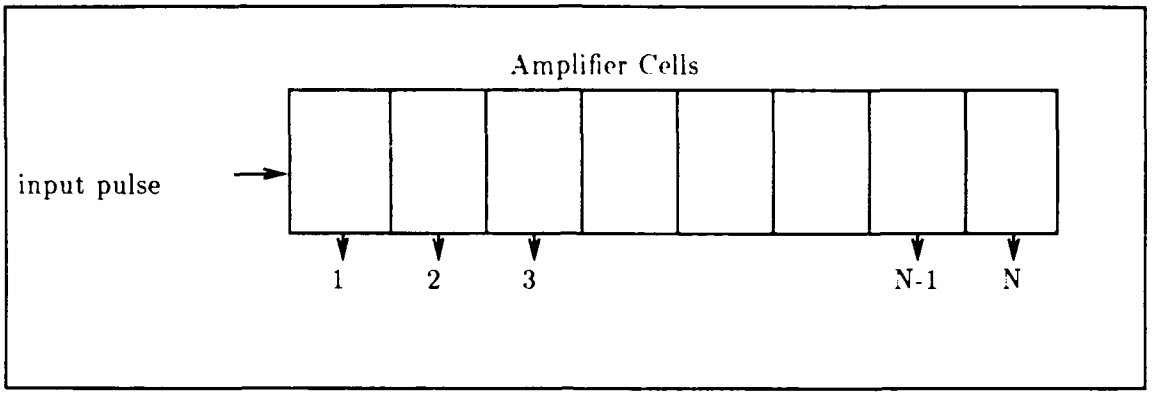

Figure 2.2. Diagram of Douglas-Hamilton model

tion for constant inversion within a cell becomes more valid. Therefore, we would expect increased accuracy in the calculation. Surprisingly, this was not the case for their model. Their predictions for flux intensity were exactly the same over time, whether N = 1 or N = 20. They also assert that:

> This independence of N holds for a completely saturated and a completely unsaturated amplifier, as well as for the case where the amplifier saturates somewhere along its length. (4:78)

The explanation given is that local gain is only a function of photon density. That is, their rate constants are reduced to zero. More information on amplifier output without gas kinetics appears in the validation chapter.

The discussion of their model does not explicitly define the manner in which the input pulse is divided to "fit" into each cell at each time interval. In Stone's model, the data for the output pulse is already divided into time units based on his code's time step (h1) and the average lifetime of a photon within a particular resonator (tcav). For this reason, we cannot arbitrarily choose any value for N amplifier cells. In this model we will use the relationship $x = ct$ to define not only the position in the amplifier, but also the length of each cell. In this equation, c is the speed of light in the medium and t is a unit of time defined by the number of tcav time units that have elapsed. For example, if tcav

is 10 nanoseconds and h1 is 0.1, the length of one amplifier cell will be 0.3 meters. If the length of the amplifier is three meters, then it will be divided into 10 cells.

2.2.1 Basic Amplifier Equation. If we allow j to be the time unit under consideration and k to represent a particular cell within the amplifier, the equation for photon density growth from one cell to the next cell is:

$$P_{(j+1,k+1)} = P_{(j,k)} e^{(g_{(j,k)}-\alpha)L} \tag{2.1}$$

where P is the number of photons per cubic meter, g is the gain coefficient, α is the loss per unit distance due to scattering and possible absorption by non-active constituents in the laser medium, and L is the length of the amplifier cell. The gain coefficient is the product of the population inversion and σ, the stimulated emission cross section. The expression $e^{(g-\alpha)L}$ is also known as the small-signal gain and will be represented by the symbol, G.

The population inversion ($Nversion_{(j,k)}$ in the model) is calculated using a slightly modified version of Stone's numerical method. Basically, the normalization terms have been removed and the photon density growth now occurs outside the Runge-Kutta integrator. It must be emphasized here that the validity of this integration method has already been established, and the validation portion of this modeling effort will only deal with the actual amplification process (7). As in Stone's code, the stimulated emission cross section is calculated in this manner:

$$\sigma = \frac{F_{u(J=19)}(A_{21})c^2}{4\pi^2(\nu)^2\Delta\nu_p} \tag{2.2}$$

where A_{21} is the Einstein coefficient of spontaneous emission,[2] ν is the frequency of the $J19 - J20$ [P(20)] transition, $\Delta\nu_p$ is the linewidth of the emission, and $F_{u(J=19)}$ is the fraction of molecules in the 001 vibrational level that are in the $J = 19$ rotational level (7:2535). In the model, $F_{u(J=19)}$ is calculated as part of the Boltzmann distribution for the rotational levels. The distribution is based on the parameter for initial temperature. We will assume the rotational thermalization rate to be high enough to maintain this Boltzmann distribution throughout the amplification process. Rooth has shown the thermalization

[2] A_{21} will be described in more detail in the ASE section.

time to be less than one nanosecond (19:108). So, as long as the input pulse does not saturate the gain in a nanosecond, we will not need to consider rotational nonequilibrium.

The linewidth of the emission, $\Delta\nu_p$, is calculated as a function of gas mix, temperature, and pressure using an equation adapted from Witteman (25:61):

$$\Delta\nu_p = 7.58(\Phi_{CO_2} + 0.73\Phi_{N_2} + 0.64\Phi_{He} + 0.32\Phi_{H_2} + 0.38\Phi_{H_2O})Pres\sqrt{\frac{300}{Temp}} \qquad (2.3)$$

where Φ represents the percentage of a gas in the mix. For typical gas mixes, the calculation is valid at pressures ($Pres > 0.015$ atm) where collision broadening dominates and the lineshape is approximately Lorentzian (22).

2.2.2 Additional Calculations. Before we look at the iterative steps of the amplification process, two more calculations will be described. First, the input data must be converted from megawatts/liter into photons per cubic meter. The derivation of this conversion constant (Factor1) appears in Appendix B. Second, each input unit is modified by the transmissivity of the window as it passes through the entrance and exit of the amplifier. Typically, practical devices have windows with anti-reflective coatings. Anti-reflective coatings can be designed to allow more than 98 percent of incident light, within a particular range of frequencies, to pass through the window (17).

2.2.3 Step-by-Step. The amplification process, as modeled here, is a two-step process nested in two loops. The outer loop is for the current time step. The inner loop is for the current cell under consideration. Within this loop both amplification steps occur. First, a small-signal gain is calculated for that cell using its current population inversion. If the photon density in that cell was greater than zero at the previous time interval, then the new inversion will reflect changes due to pumping, collisional relaxation, *and* spontaneous emission. Next, using Equation 2.1, the photon density is calculated for the next cell at the next time unit. These steps are done for each cell before the next cell is considered. Only after the calculations are completed for all cells (k) is the next time (j) unit considered.

Initially (time unit $j = 0$), all values for photon density ($P_{(0,k)}$) are set to zero and an input power value for each time step is stored in a file called FileInput. Now let's look

at what happens in the first amplifier cell:

- At $j = 0$.
    1. The small-signal gain is calculated using the population inversion determined by the Runge-Kutta subroutine.
    2. Using Equation 2.1, the photon density is calculated for the next cell. In this case, the value will be zero because the value for photon density in cell 1 was initialized to zero.
    3. Next, the first value from FileInput is multiplied by both Factor1 and the window transmissivity. At this point, it is the photon density value in cell 1 for $j = 1$.
- These steps are repeated for all amplifier cells.
- At $j = 1$.
    1. The small-signal gain is recalculated for cell 1.
    2. Using Equation 2.1, the first value from FileInput is "amplified" to become the value for photon density in cell 2 at $j = 2$.
    3. Now the next value from FileInput is read in and modified to become the photon density value in cell 1 at $j = 2$.

From here let's move on to a point in time where the first value from FileInput is just about to enter the last cell:

- At j = end - 1.
    1. Following all of the other cells, the small-signal gain is calculated for the last cell.
    2. Using Equation 2.1, an *output* value is calculated. In this case, the value is zero.
    3. Finally, the first value from FileInput arrives.
- At j = end.

1. Again, the small-signal gain is calculated for the last cell.
2. The first value from FileInput is "amplified" one more time and becomes the output value for $j = \text{end} + 1$. As noted earlier, the length used for amplification by the last cell may be shorter than the rest of the cells. This fact is included in the calculation. However, the units used for time are not as flexible. So, the data table may list a slightly longer time-to-exit than actually occurs.
3. To finish the calculation for this output slice, it must be multiplied by the window transmissivity and converted from photons per cubic meter to megawatts.

2.2.4 Effects to be Modeled. Two important effects illustrated by this model are gain saturation and pulse sharpening. Saturation of amplifier gain sets a fundamental limit on the abilities of the laser system. As noted earlier, the process of amplification reduces the population inversion. When the populations of the two coupled levels have been equalized, the gain is saturated. Figure 2.3 shows the distribution of gain after a pulse has propagated through the amplifier. In this case, only the last cell has been completely saturated. A natural consequence of saturation is pulse sharpening. For example, Figure 2.4 compares a square pulse before and after amplification. Prior to amplification, the energy was equally distributed throughout the pulse's duration. After amplification, the pulse has most of its energy located near the leading edge. Figure 2.5 illustrates pulse sharpening during the amplification of oscillator pulses. Curve A represents the amplifier input. Curves B and C are the outputs of amplifiers with lengths x and $2x$, respectively.

2.3 ASE Fundamentals

In the amplification process presented above, the primary cause of energy loss from the population inversion is stimulated emission. So far, the only source term for these emissions is the input pulse. Other source terms that will be modeled are spontaneously emitted photons. These photons are emitted in all directions, but only those propagating axially—either forward or backward—will contribute to a significant decrease in the population inversion. The bidirectional increase in ASE intensity is shown in Figure 2.6. In high-gain amplifiers, ASE output can be both intense and relatively narrow in bandwidth.

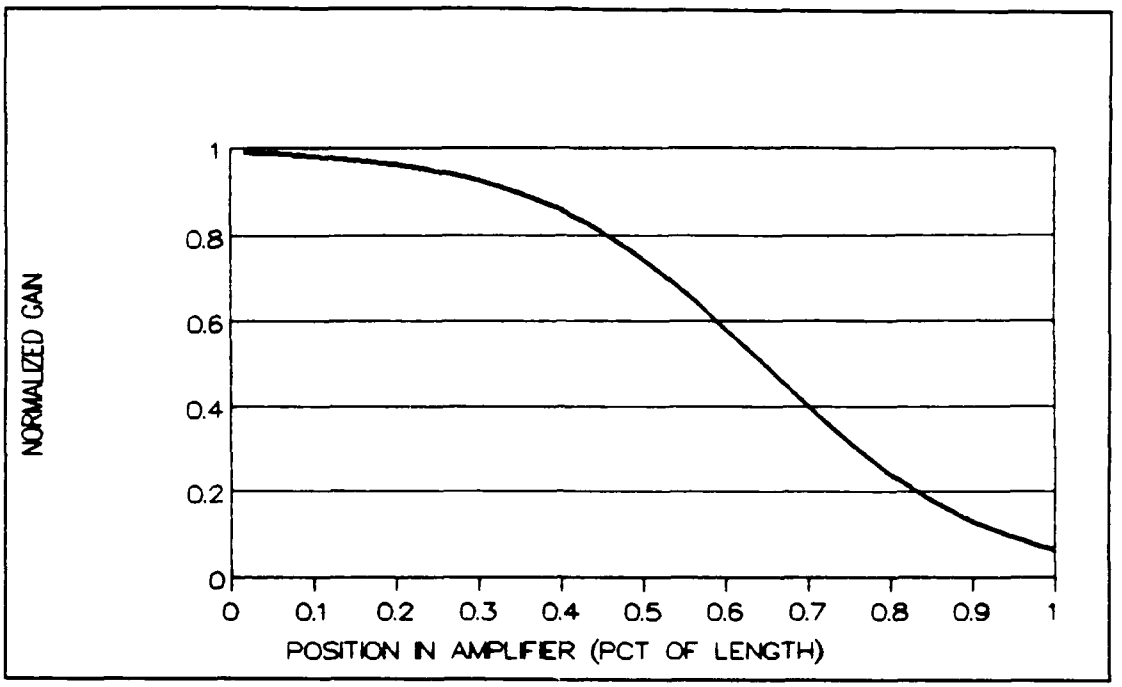

Figure 2.3. Typical gain profile after a pulse has been amplified

However, because this output will not have the spectral qualities of an oscillator input beam, it is useless in a laser radar system. Because this energy extraction is counterproductive, amplifiers must be designed to avoid unnecessary losses to ASE. Essentially, three parameters determine whether or not ASE will significantly limit the output of the laser amplifier:

1. Population of the upper vibrational level.
2. Solid angle for amplification.
3. Gain coefficient.

2.3.1 Population of the Upper Vibrational Level. Molecules in an excited energy state (E_1) generate photons by spontaneously dropping to a lower energy state (E_0). The laser transition for CO_2 molecules is from v = 001 to v = 100. This transition can occur between any one of over fifty rotational level pairs associated with the excited v = 001 level. Each of these rotational levels emits photons at a unique frequency. In addition, each

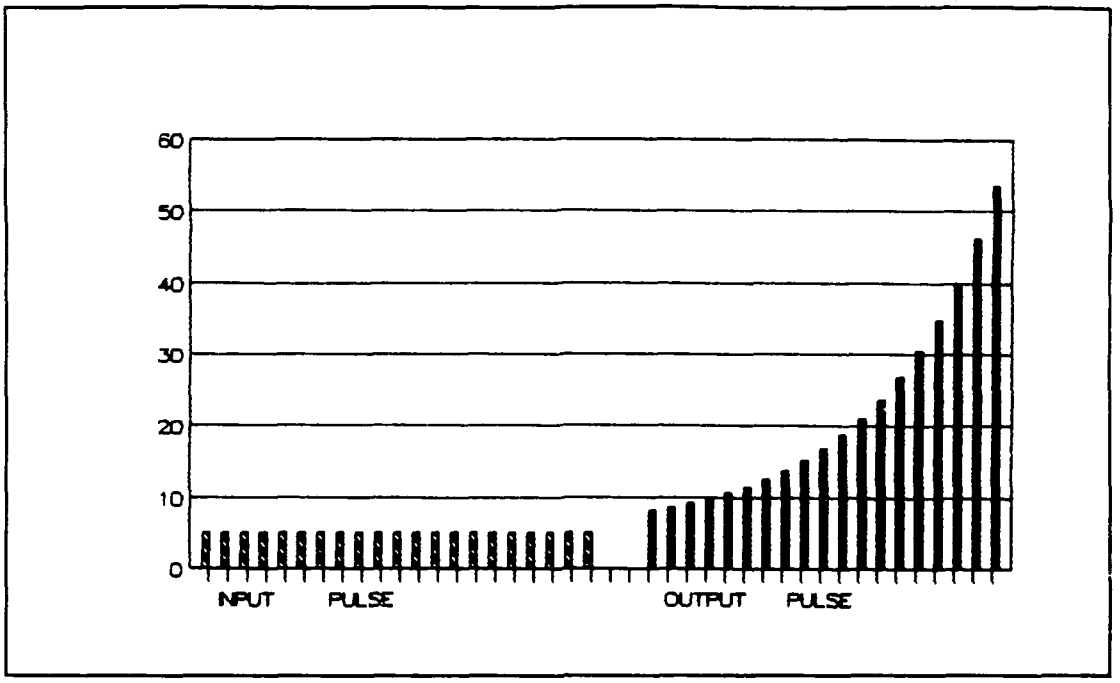

Figure 2.4. Amplification of a square input pulse

level emits photons at a different rate. The rate at which these emissions occur is described by the Einstein coefficient of spontaneous emission, A_{21}. For example, the transition from $v = 001$ to $v = 100$ on the $J = 19$ rotational line has a value of 0.194 $\sec^{-1}$ (8:536). In our model, we use the product of this constant, the population density of its rotational level, and the time step to generate the ASE photon density, at a particular frequency, during one time step. Since A_{21} is a constant, and $F_{u(J=19)}$ is assumed to be constant,[3] the parameter that determines how many photons will be spontaneously emitted is the population density of the upper vibrational level, $v = 001$. In the model the equation is:

$$\text{ASE}dt = y0_{(1,k)}(F_{u(J=19)})(A_{21})(tcav \times h1) \tag{2.4}$$

[3]The model does not recalculate temperature after each iteration, so $F_{u(J=19)}$ is assumed to be constant. Because the validity of this assumption depends on the rate at which temperature increases in the cavity, this model is valid only for pulses with relatively short durations.

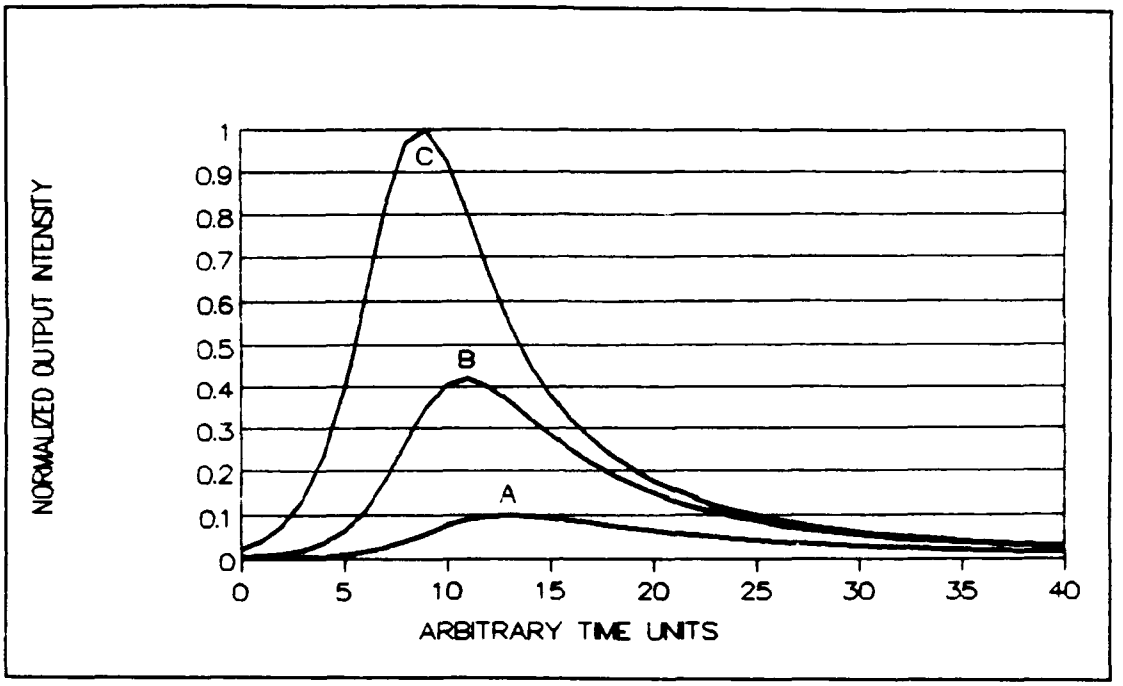

Figure 2.5. Amplification of an oscillator's output pulse (curve A)

where "ASEdt" represents the density of photons spontaneously emitted during one time step and $y0_{(1,k)}$ is the population density of the upper vibrational state. By multiplying by $F_{u(J=19)}$, we are calculating the population density of only those photons emitted as a result of $J19 - J20$ transitions.

In a conservative approximation, we will calculate the ASE density at line center. Then, to account for all of the other emissions, we divide that photon density by $F_{u(J=19)}$. In this way, we treat each emission line as if all the photons on it are amplified at line center gain. Our approximation is conservative because the gain at line center is slightly greater than the gain at the other transition frequencies (16:31). Therefore, we overestimate the effect of ASE on the population inversion.

To reemphasize this effect, consider that with higher gain at line center more photons will be generated at that frequency. Since amplification is an exponential process, photons at line center "win the competition" for the gain and dominate the ASE output. Thus, ASE has a narrow bandwidth. In fact, the higher the gain in the system, the narrower its

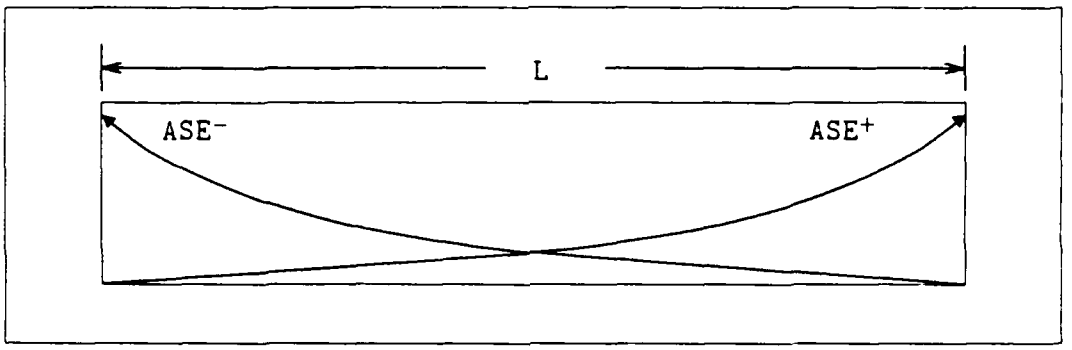

Figure 2.6. Relative intensity for ASE traveling in both directions

line shape gets (24:181-182). Figure 2.7 compares our approximation of the ASE lineshape to its theoretical line shape.

To compare ASE to the previous amplifier analysis, one can think of each cell as an input window. At each time interval, each cell contributes more photons to the ASE "pulse". Some of the ASE photons will travel the same direction as the oscillator input pulse. Assuming isotropic emission, an equal portion will travel the opposite direction. "ASE^+" will be used to refer to the copropagating photons and "ASE^-" will be used to refer to the counterpropagating photons.

2.3.2 Solid Angle. Of the photons traveling axially, only a fraction of them will make it out of the amplifier. In our model, we assume these photons are the only ones that significantly affect the gain in the amplifier. If we neglect wall reflections, this fraction can be approximated in terms of solid angles. The photons are emitted into a solid angle of 4π steradians. The fraction traveling in the proper direction is $\Omega/4\pi$, where Ω is the solid angle subtended from a point in the amplifier to the appropriate wall. There are two solid angles for each position in the amplifier, one for ASE^+ and one for ASE^-. For amplifiers with circular cross sections, Ω is given by:

$$\Omega = \int_0^{\theta} 2\pi \sin\theta d\theta \tag{2.5}$$

where θ is the angle illustrated in Figure 2.8 (21:528-529). The solution to the integral has

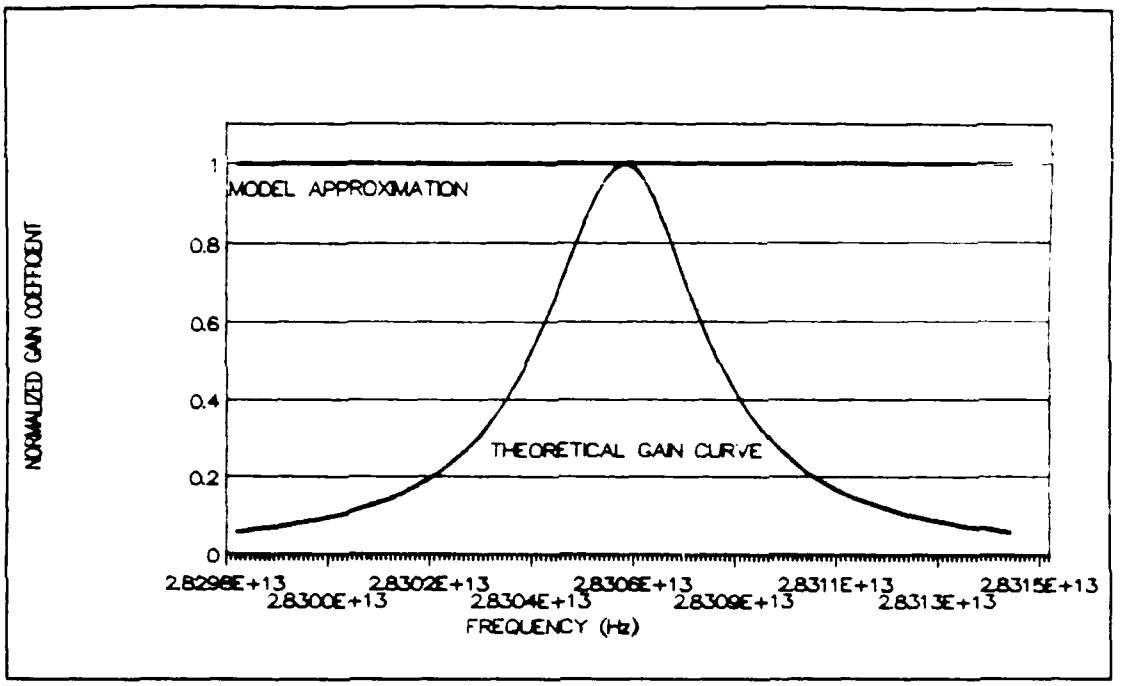

Figure 2.7. Comparison between the theoretical and the modeled ASE lineshape

the forms:

$$\Omega^{+} = 2\pi\left(1 - \frac{L - x}{\sqrt{(L-x)^2 + (d/2)^2}}\right) \tag{2.6}$$

$$\Omega^{-} = 2\pi\left(1 - \frac{x}{\sqrt{x^2 + (d/2)^2}}\right) \tag{2.7}$$

for ASE^{+} and ASE^{-}, respectively. In these equations, L is the length of the amplifier, x is the axial position, and d is the diameter of the circular aperture (1:2033-2034). Clearly, the fraction of photons that contribute to ASE is a function of amplifier length and diameter.

2.3.3 Gain Coefficient. Thus far, we have an equation for calculating the amount of ASE each cell adds at each time interval and an equation for the fraction of those photons having a direction that allows them to contribute to the ASE output. With the addition of the small-signal gain term, we arrive at the equations used for propagating ASE from

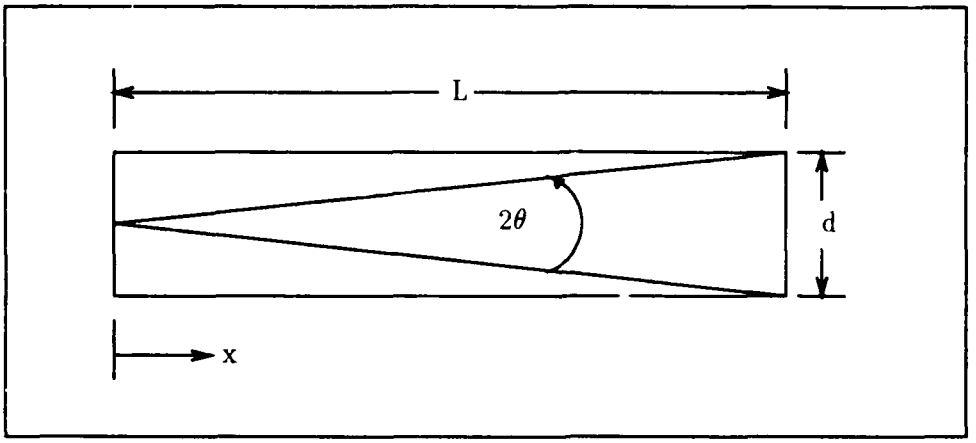

Figure 2.8. Angle defining solid angle limits of integration

cell to cell:

$$\mathrm{ASE}^{+}_{(j,k)} = \mathrm{ASE}^{+}_{(j-1,k-1)} G_{(j-1,k-1)} + (A_{21})(y0_{(1,k)}) \left(\frac{\Omega^{+}}{4\pi}\right) \tag{2.8}$$

$$\mathrm{ASE}^{-}_{(j,k)} = \mathrm{ASE}^{-}_{(j-1,k+1)} G_{(j-1,k+1)} + (A_{21})(y0_{(1,k)}) \left(\frac{\Omega^{-}}{4\pi}\right) \tag{2.9}$$

where the terms $k-1$ and $k+1$ refer to the cell where the ASE is coming from.

Using Equations 2.6, 2.7, 2.8, and 2.9, the iterative steps for computing the ASE output are the same as the steps describing the amplification of a radar pulse. All of these equations are performed for each cell at one time step before the next time step is considered. In the main program the photon densities for ASE and the radar pulse are determined separately. This must be done because the counterpropagating wave, ASE^{-} uses the population inversion from the $k+1$ cell to determine the gain used to amplify its intensity. However, in the Runge-Kutta subroutine, it is their combined effect that drives the population inversion toward saturation.

In terms of the photon density required to saturate the ends of the amplifier, the principle ASE parameters are limited in this way:

$$e^{gL} - 1 < \frac{4\pi}{\Omega} \tag{2.10}$$

where Ω is a function of length and diameter. The details of Equation 2.10 will be discussed in Appendix C. The simplest approximation for Ω is A/L^2, where A is the cross-sectional area of the amplifier and L is its length (14:399). For circular cross sections, the equation for preventing saturation is now:

$$e^{gL} - 1 < \frac{16L^2}{d^2}. \tag{2.11}$$

Figures 2.9, 2.10, and 2.11 illustrate these limitations graphically. Figure 2.9 shows how sensitive diameter is to changes in initial gain and length. Similarly, Figure 2.10 shows how sensitive length is to changes in initial gain and diameter. Figure 2.11 shows how length and diameter can limit the initial gain.

2.4 Reflected ASE

The effect of ASE on amplifier gain is even more significant if we consider the reflectivity of the cavity windows. Now the amplifier acts like an oscillator, and the intensity of ASE grows until the gain drops off significantly. Thus, window reflectivity is an important design parameter. In fact, analysis has shown that decreasing window reflectivity is the most effective way to circumvent ASE limitations on amplifier gain (2:147). The following numeric example will demonstrate the importance of window reflectivity. We start with 1×10^9 ASE photons at one end of a 15-meter amplifier with a constant gain profile. The gain coefficient at line center is 100 percent per meter. Fifty nanoseconds later the ASE photons have traversed the cavity and have grown to 3.3×10^{15}. If only a tenth of one percent is reflected, there will be 3.3×10^{12} photons headed back toward the other end of the cavity—over 3000 times the number we had initially.

2.4.1 Equations for Reflected ASE. Not all ASE that is reflected will propagate the entire length of the amplifier. We should recall that the photons had to be emitted into a small solid angle to make it to the reflecting surface. Additionally, this solid angle varied depending on the emission's position within the amplifier. If we think of the solid angle as an angle of divergence, it is obvious that an even smaller angle Ω' is required for ASE to be able to reflect off one end and exit the opposite end. Figure 2.12 shows these two angles

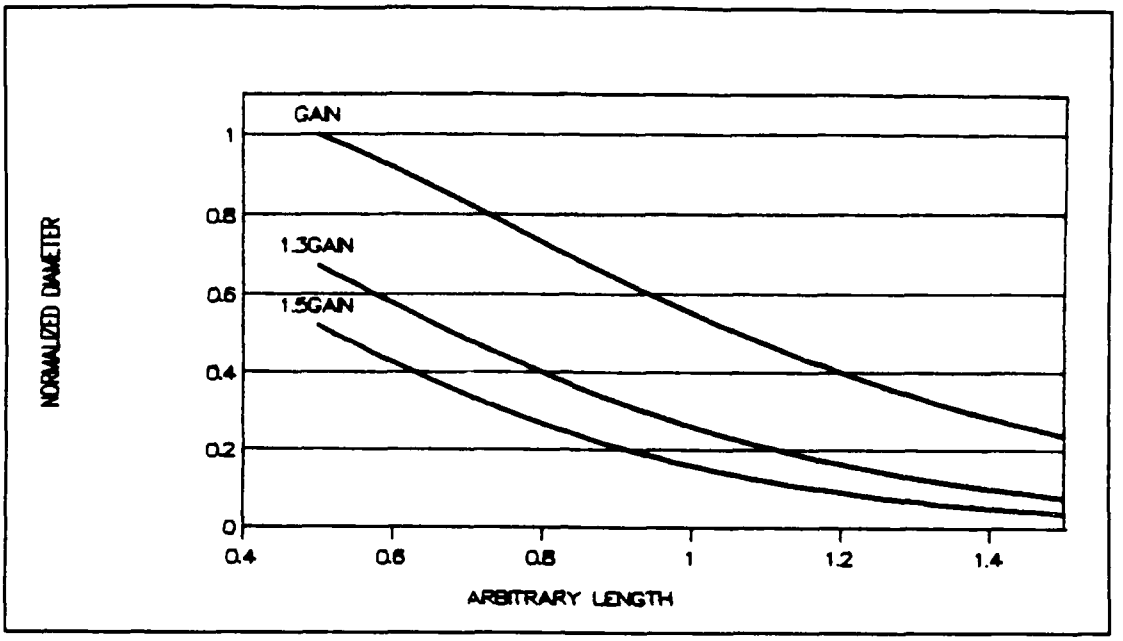

Figure 2.9. ASE parameter trends in the saturation limit: Gain vs Length

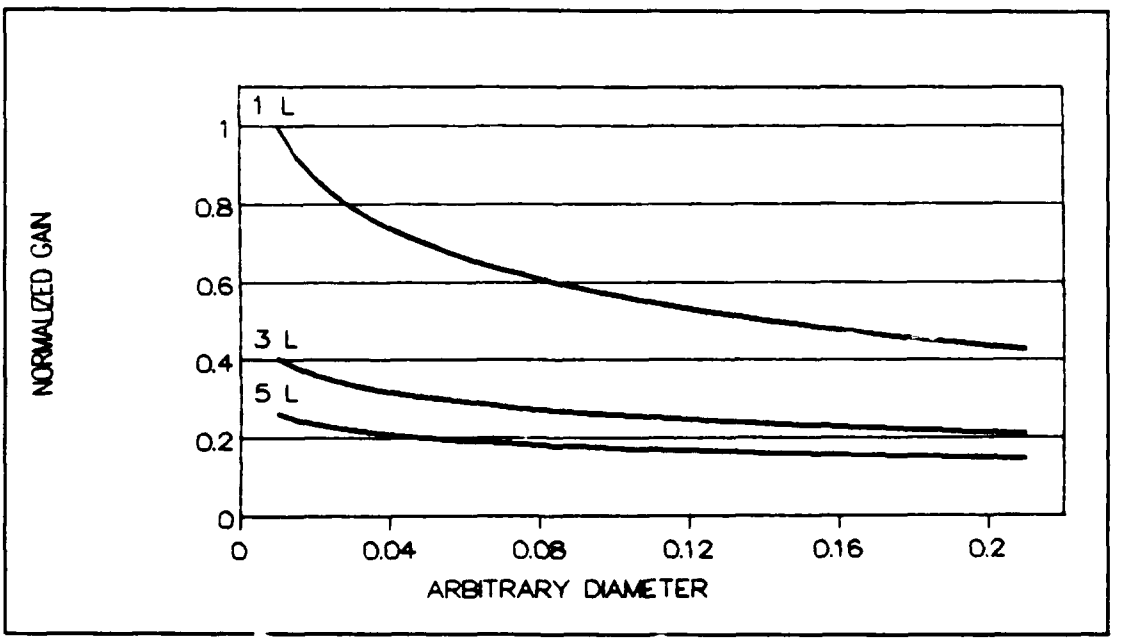

Figure 2.10. ASE parameter trends in the saturation limit: Gain vs Diameter

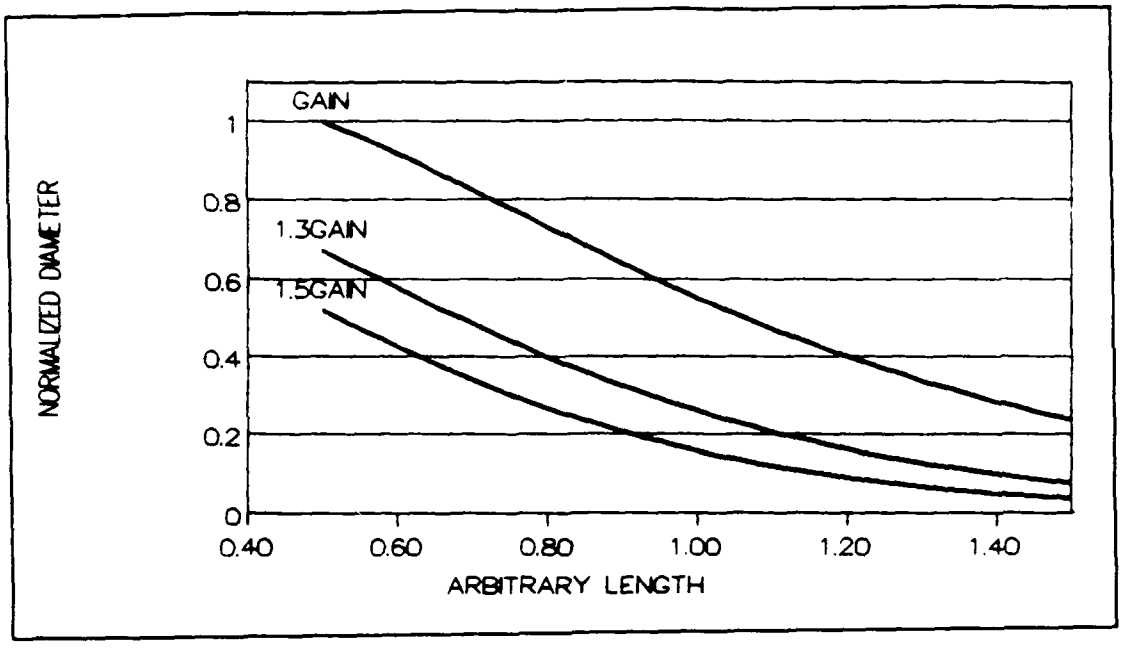

Figure 2.11. ASE parameter trends in the saturation limit: Diameter vs Length

of divergence by unfolding the reflected half of the ASE path. Both angles increase for emission positions closer to the end of the amplifier. In the model, each cell's contribution to the ASE output includes a calculation for the fraction of photons that are emitted into Ω'. The equations for this "reflectable fraction"are:

$$\Omega'^{+} = \frac{\pi(d/2)^2}{(2L-x)^2}\frac{1}{\Omega^{+}} \tag{2.12}$$

$$\Omega'^{-} = \frac{\pi(d/2)^2}{(L+x)^2}\frac{1}{\Omega^{-}} \tag{2.13}$$

for reflected ASE^{+} (ASE_r^{+}) and reflected ASE^{-} (ASE_r^{-}), respectively (1:2039). The equations for their amplification are:

$$ASE^{+}_{r(j,k)} = \Omega'^{+}ASE dt + ASE^{+}_{r(j-1,k-1)}G \tag{2.14}$$

$$ASE^{-}_{r(j,k)} = \Omega'^{-}ASE dt + ASE^{-}_{r(j-1,k+1)}G \tag{2.15}$$

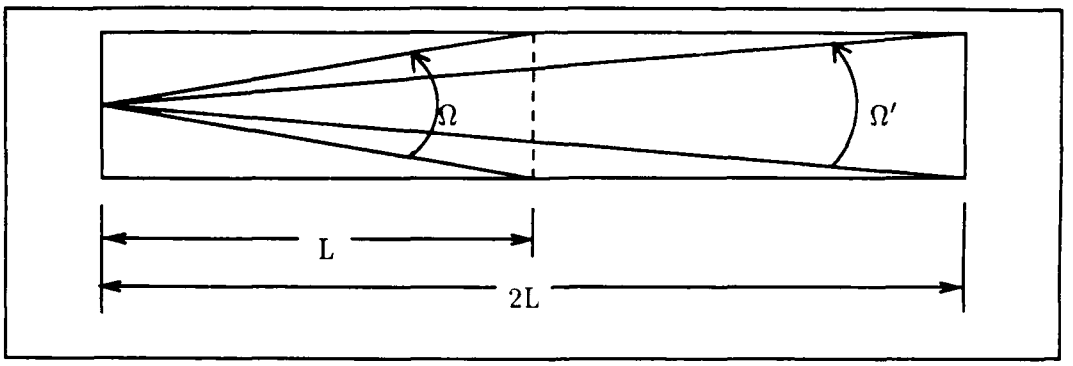

Figure 2.12. Maximum divergence angles for ASE (Ω) and reflected ASE (Ω')

These values will be amplified alongside ASE^+ and ASE^-. However, they will not affect the population inversion. They are monitored strictly to determine the amount of ASE that will reenter the medium and contribute to the power output at the opposite end.

For example, let us consider the end of the medium where $x = L$. Without a reflected contribution, ASE^- has a population density of $A_{21}y0_{(1,k)}\Omega^-/4\pi$ (ASEdt in the code). Reflection adds to ASE^- the present value for ASE_r^+ multiplied by the window reflectivity. The only remaining calculation to be done is to determine what fraction of ASE_r^+ can now become a source for ASE_r^-.

2.4.2 Combining the ASE Terms. Figure 2.13 shows that the ASE_r^+ photons that arrive at the end of the cavity have a divergence angle between (small-angle approximations) d/L and $d/2L$. The larger angle includes those photons generated close to the reflecting surface and the smaller angle includes those generated near the end of the amplifier. To continue our conservative approach, we will assume all of the photons arrive with the smaller divergence angle. With this assumption, Figure 2.14 shows that $\frac{4}{9}$ of the ASE_r^+ photons can be added to ASE_r^-. These photons, reduced by the reflectivity of the first window will be reflected one more time before exiting the amplifier. In effect, we monitor two reflections for any cell's ASE photons. We assume further reflections have a negligible effect on the overall ASE intensity. Thus, the equations for ASE^- and ASE_r^- in the last

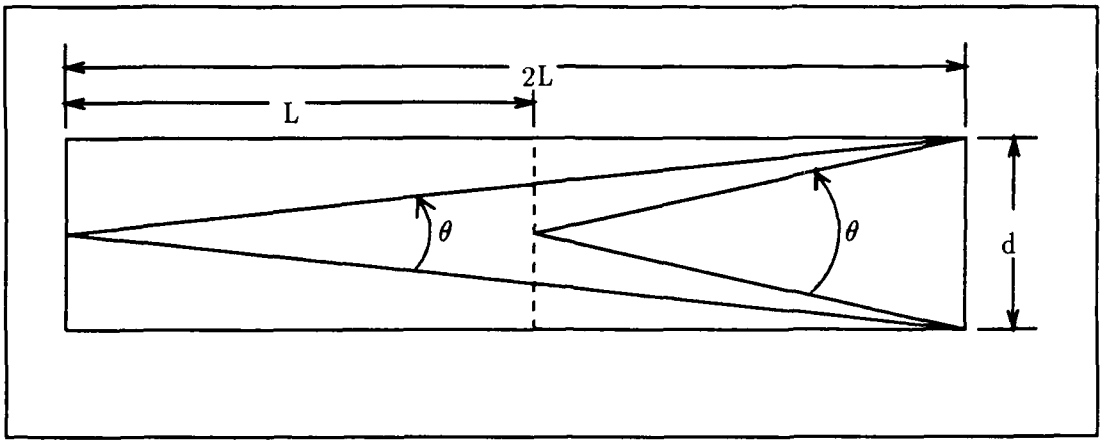

Figure 2.13. Range of divergence angles for reflected ASE exiting the amplifier

amplifier cell are as follows:

$$\mathrm{ASE}^{-}_{(j,k)} = \mathrm{ASE}dt + \Re\left(\mathrm{ASE}^{+}_{r(j-1,k)}\right) \tag{2.16}$$

$$\mathrm{ASE}^{-}_{r(j,k)} = \Omega'^{-}(\mathrm{ASE}dt) + \Re\left(\mathrm{ASE}^{+}_{r(j-1,k)}\right)\left(\frac{4}{9}\right) \tag{2.17}$$

with $\Re$ representing the reflectivity of the cavity window. Parallel equations are used to calculate ASE^{+} and ASE^{+}_{r} in the first cell.

Putting all the ASE equations together, certain phenomena are expected in simple cases where gain is independent of gas kinetics. If the reflectivity is zero, the ASE output intensity will increase until all points inside the amplifier are contributing to the output. The time period for this increase is the time required for a photon to travel the length of the amplifier. After this time, the intensity remains relatively constant, decreasing as the population inversion is depleted. If the reflectivity is greater than zero, the population inversion is depleted much more rapidly. With a reflected contribution to ASE at the ends of the amplifier, the ASE intensity continues to grow until the gain is saturated.

2.5 Reflected Input Pulse

The last loss term included in this model is also a result of window reflectivity. Like ASE, the input pulse itself can be reflected back into the amplifier and reduce the

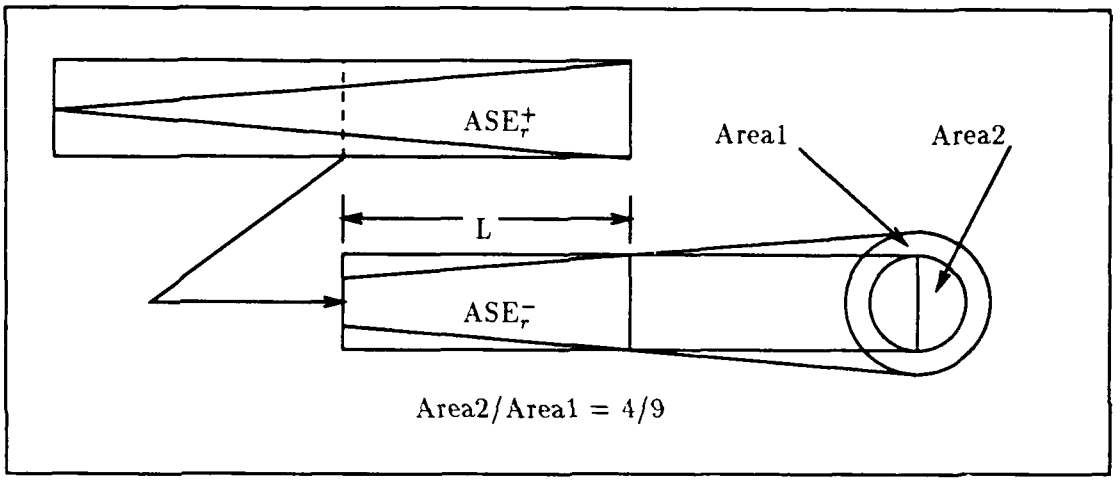

Figure 2.14. Fraction of ASE^+ that can contribute to ASE^-

population inversion. However, this reflection tends to dampen itself out rather than grow exponentially. For example, let's say that an input intensity of 100 W/cm^2 exits the amplifier with an intensity of 500 W/cm^2. We'll assume there are no anti-reflective coatings, so we can expect up to four percent reflection. Therefore, 20 W/cm^2 will reenter the cavity. Though this is only $\frac{1}{5}$ the amount we started with, it cannot be neglected. It will still affect the gain that the remainder of the pulse experiences.

Modeling this phenomena is much simpler than modeling reflected ASE. Because all of the photons in the pulse are traveling the same direction there are no solid angles to calculate. Assuming the photons leave the amplifier only through one of the windows, the following five equations describe their cyclic flow. We start with the initial reflection:

$$P^-_{r(j,k=last)} = \Re\left(P_{(j-1,k=last)}\right). \tag{2.18}$$

Now we have a reflected pulse traveling in the negative direction. It is amplified according to:

$$P^-_{r(j,k)} = \left(P^-_{r(j-1,k+1)}\right)\left(G_{(j-1,k+1)}\right) \tag{2.19}$$

until it reaches the beginning of the amplifier where it is reflected once more:

$$P^{+}_{r(j,k=1)} = \Re\left(P^{-}_{r(j-1,k=1)}\right). \tag{2.20}$$

Again, it is amplified as it propagates in the positive direction:

$$P^{+}_{r(j,k)} = \left(P^{+}_{r(j-1,k-1)}\right)\left(G_{(j-1,k-1)}\right). \tag{2.21}$$

Finally, the pulse arrives at the end of the amplifier where it is reflected together with any of the input pulse that may still be passing through the amplifier:

$$P^{-}_{r(j,k=last)} = \Re\left(P^{+}_{r(j-1,k=last)}\right) + \Re\left(P_{(j-1,k=last)}\right). \tag{2.22}$$

The last four equations are then used for the remaining cycles to calculate the gain reducing terms, P_r^+ and P_r^-.

2.6 Summary

In addition to gas kinetics and electrical pumping, this model simultaneously monitors four other gain-reducing terms. In order of appearance, they are: ASE, reflected ASE, the input pulse, and its reflection. These terms are added in the Runge-Kutta subroutine to form a single value for the photon density. This value is used to calculate new populations for the $v = 001$ and $v = 100$ states of CO_2 in each cell for each time interval. After the populations are returned from the subroutine, the gain in each cell is determined. The gain is then used to calculate the growth of each of our monitored terms. The next chapter describes the validation of each of these modeled processes.

III. Validation

3.1 Amplification

The validation process for a computer model begins with a series calculations to verify each equation and algorithm. Once the step-by-step correctness is established, the model is ready for direct comparison to experimental results or a theoretical comparison to results calculated with an analytical solution. One advantage of an analytical solution over published experimental results is the ability to freely adjust the input parameters. By varying the inputs over a wide range, it is possible to determine trends in the errors produced by the model. These trends establish the boundaries within which the model produces reasonable output. To validate our amplifier model, we used the analytic equations derived by Frantz and Nodvik for the amplification of a "square" pulse[1] (5:2348).

3.1.1 Conditions for Closed Form Solution. To arrive at their solution, Frantz and Nodvik used four simplifications. First, they assume a two-level system, meaning the sum of the number densities for the upper and lower states is constant. Second, they neglect any frequency dependence by assuming the input beam to be monochromatic. Third, they neglect spontaneous emissions. With this assumption, only the input pulse plays a role in changing the population inversion. Fourth, they assume the population inversion varies only one dimensionally and that it is initially uniform across the amplifier.

To duplicate these conditions, our model was both enhanced and constrained. The enhancement was a new set of input parameters to create "square" pulses and allow any initial gain setting. We already assume line center operation, so no adjustment was necessary for their monochromatic assumption. The remaining assumptions were duplicated by constraining our rate equations. In the equation for ASE, A_{21} was set to zero, thus eliminating any spontaneous emissions. In the equations for collisional relaxation, the degeneracy ratio was set to one and all of the rate constants and pump terms were set to zero. In effect, we turned off the kinetics and allowed the population inversion to be reduced only by the stimulated emission process.

[1] "Square" refers to constant amplitude with rise and set times of zero.

The result of all these adjustments was a clean validation environment where the differences between our results and those obtained with the Frantz-Nodvik equations were not related to pumping, collisional relaxation, or ASE. Also, we were able to compare both long and short pulses. If we had left the kinetics on, we would have been limited to pulse durations on the order of tens of nanoseconds because the Frantz-Nodvik solution is "justified (only) during times small compared to the radiative lifetime of the excited state"(5:2346). Furthermore, such a time scale would have required consideration of nonequilibrium among the rotational levels of the excited state. This consideration is beyond the scope of our model. So, to validate our model on a theoretical level, we used a clean, "kinetic-less" environment.

3.1.2 Comparison to the Frantz-Nodvik Solution. The Frantz-Nodvik equation for a square pulse traversing an amplifier with initially uniform gain expresses photon density as a function of time and position in the amplifier:

$$n(x,t) = \frac{n_0}{1 - [1 - \exp(-\sigma\Delta_0 x)]\exp[-2\sigma\eta(t - \frac{x}{c})/\tau]} \tag{3.1}$$

where n is the photon density, Δ_0 is the initial population inversion, η is the total number of photons per unit area of the pulse, and τ is the pulse duration (5:2348). This equation was used to compare amplifier output on a point-by-point basis.

First, we simply compared outputs for $t = L/c$, where L is the amplifier length. This is the instant in time when the leading edge exits the amplifier. As mentioned before, the leading edge is the only part of the pulse to see the full inversion. As expected, both the equation and model had the leading edge amplified exactly by e^{gL}. Figure 3.1 compares the outputs for $t > L/c$. The curves were generated using a high-gain (160 percent per meter), one-meter amplifier and a large input pulse (6 MW/cm^2). Here we note the error between values based on integration over a few cells (the model) and an infinite number of cells (the Frantz-Nodvik equation). Both curves start at zero error.[2] The lower curve in

[2]The initial error is zero because the leading edge of the pulse experiences a constant gain profile. Therefore, its amplification is described by e^{gL}.

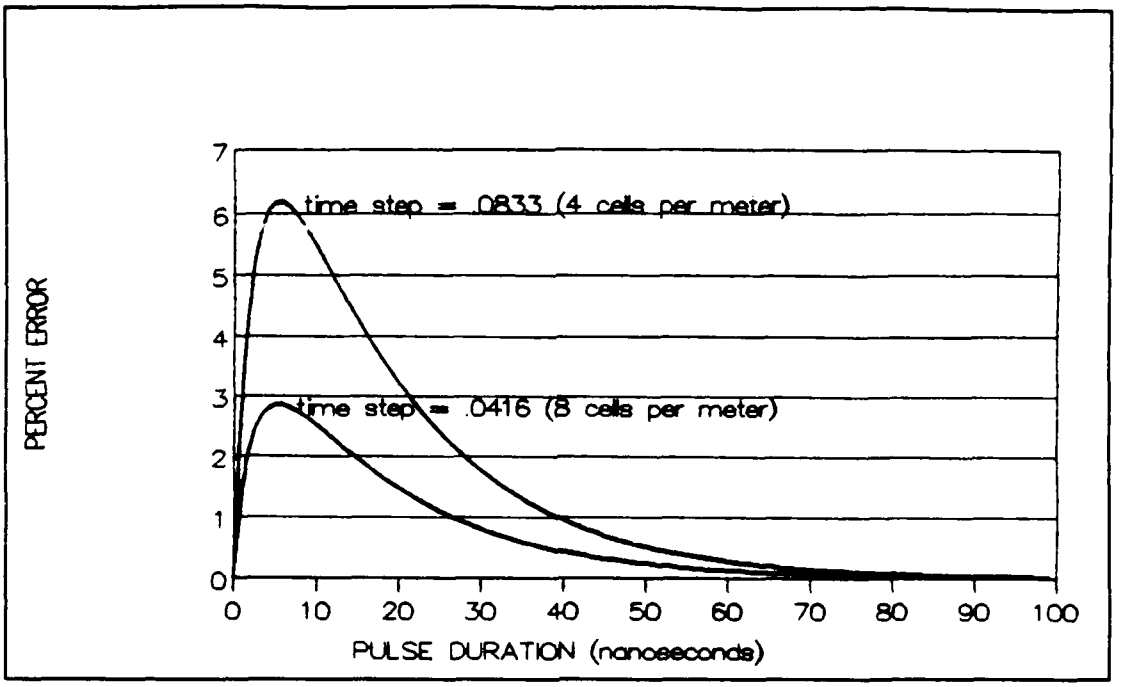

Figure 3.1. Percent error between model and Frantz-Nodvik equation as a function of time

Figure 3.1 shows the overall error reduction if the amplifier is divided into twice as many cells.

The error is due to the fact that the model only approximates the positional dependence of gain. We still have constant gain across each cell. Smaller and smaller cells are required to describe the gain profile if the gain is changing radically from point to point. Separately or together, three factors increase our model's error. Basically, they all have to do with the intensity of the pulse inside the amplifier. Obviously, if we start with a large input pulse, the gain will change rapidly. But, even if we start with a small pulse, large gain can cause the pulse to grow large enough to saturate the end of the amplifier. If we start with a small pulse and small gain, but the amplifier is very long, the same effects occur. The only way to limit errors under these conditions is to divide the amplifier into as many cells as patience and computer memory will allow.

The convergence toward zero error by both curves in Figure 3.1 is a direct result of

reduced gain. As the amplifier becomes saturated, the pulse sustains a smaller growth rate. For this limit, where every excited atom in the amplifier decays, Frantz and Nodvik have derived an equation for the energy gain. Energy gain is the ratio of the energy contained in the output and the input pulses:

$$G_E = \int_{-\infty}^{\infty} n_L(t)dt \Big/ \int_{-\infty}^{\infty} n_0(t)dt \,. \tag{3.2}$$

For a square pulse the Frantz-Nodvik equation for energy gain is

$$G_E = (\frac{1}{2\sigma\eta}) \ln\{1 + \exp(\Delta_0 \sigma L)[\exp(2\sigma\eta) - 1]\} \tag{3.3}$$

where η is the total number of photons per unit area in the pulse (5:2348). We used this equation to determine the trends in error associated with the model's premature saturation of the amplifier. Error was calculated by the equation

$$\%\text{error} = 100(\frac{G_{E_{model}} - G_{E_{analytic}}}{G_{E_{analytic}}}). \tag{3.4}$$

Using a one-nanosecond time step, data was collected for points in time where the error was at its maximum for various amplifier lengths, initial gains, and input intensities. For comparison between energy gain error and error as a function of time, the same parameters that were used to generate Figure 3.1 were used again for this trend analysis. Combining all the data we collected, Figure 3.2 illustrates a linear relationship between error and input intensity. Table 3.1 shows that the length of the amplifier is inversely proportional to the initial gain. That is, if we want to have the same error for an amplifier twice as long, we must use half of the initial gain. The different slopes of the lines in Figure 3.2 show that among the three variables, error is most sensitive to the initial gain. This is due to the increased *rate* of energy extraction associated with higher gain amplifiers. To accurately model amplifiers with higher gains, we must divide the amplifier into smaller cells by using smaller time steps. In general, the output pulses from the model will have the same peak as the analytic solution, but they will be slightly broader.

Though the model extracts the energy from the amplifier at a slightly different rate

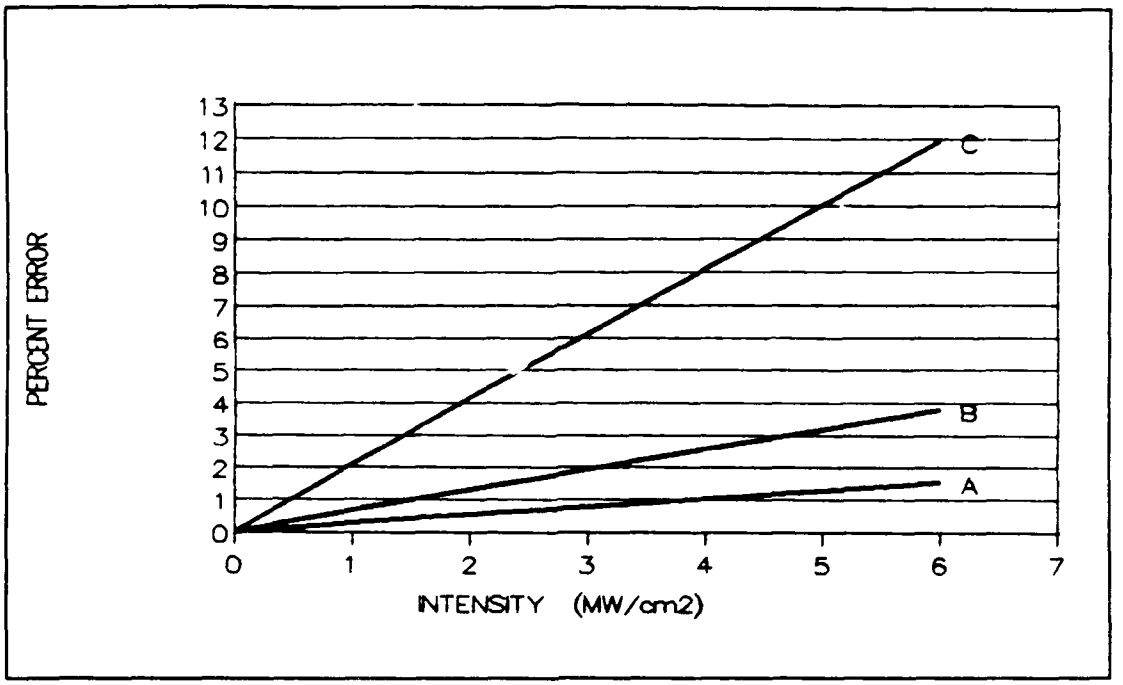

Figure 3.2. Percent error between model and Frantz-Nodvik equation as a function of input pulse intensity

Table 3.1. Data for Figure 3.2

GAIN COEFFICIENT (% per meter)			
	LENGTH		
LINE	1 meter	2 meters	4 meters
A	40	20	10
B	80	40	20
C	160	80	40

than the analytic solution, it approaches the same value for G_E in the limit where the amplifier is completely saturated. Frantz and Nodvik have shown this limiting value to be

$$G_E \sim 1 + \Delta_0 L/2\eta \tag{3.5}$$

when $2\sigma\eta \gg 1$ (5:2348). Figure 3.3 shows that as the value for $2\sigma\eta$ increases linearly, the error decreases asymptotically to zero.

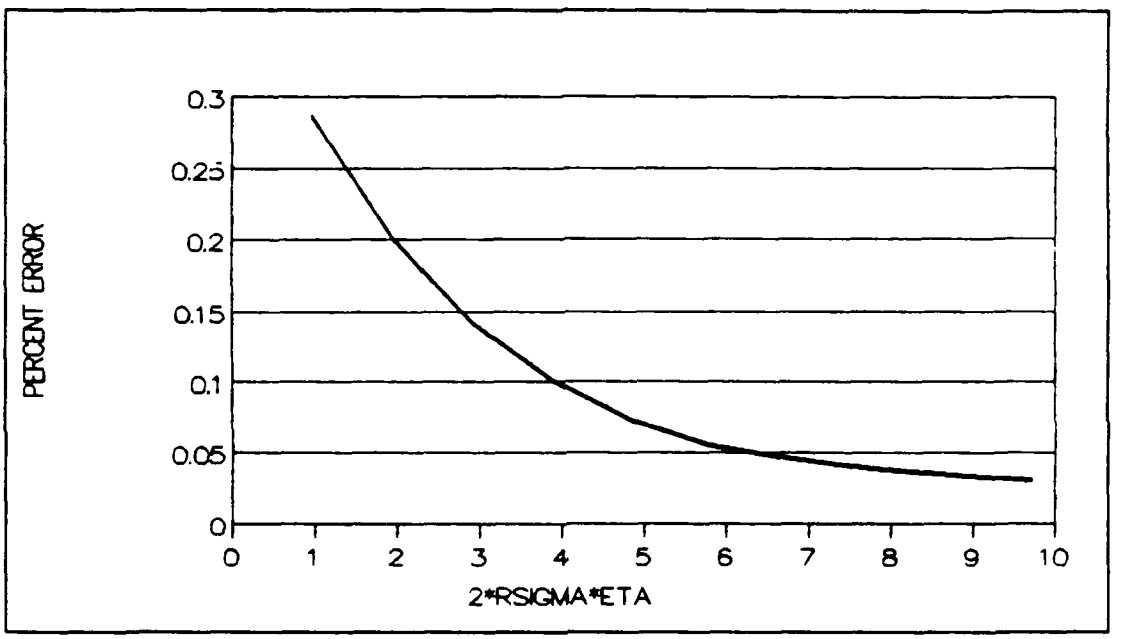

Figure 3.3. Decrease in percent error as amplifier saturates

A similar result was found in the limit for very small pulses. Pulses of "infinitesimal" width are amplified according to the exponential law. That is, they experience constant gain rather than a gain that is reduced in an intensity-dependent fashion. According to Frantz and Nodvik, a pulse is of infinitesimal width if $2\sigma\eta \ll \exp(-\Delta_0\sigma L)$ and its energy gain is described by:

$$\lim_{\eta \to 0} G_E = \exp(\Delta_0\sigma L) \tag{3.6}$$

for finite L (5:2348). By using shorter pulses and/or smaller input intensities, the model's results approached this limit.

All in all, these examples indicate that our model's results agree with Frantz and Nodvik's analytical solution. The energy gain errors are small for both very large and very small input pulses. More importantly, the time variations of the output power—the shape of the output pulse—are consistent with those calculated with the Frantz-Nodvik equations. We have found that this consistency depends on the rate at which the gain is changing. The users of this model can use Figure 3.2 as a guideline to estimate the model's errors. They should also keep in mind that using a smaller time step (more amplifier divisions) can also improve the model's accuracy.

3.2 ASE

Now that we have established the validity of our amplifier model, we can use it as the basis for validating our ASE calculations. For ASE, each cell is an input window. During each time step, each cell emits a group of photons into the cavity. As these groups propagate from cell to cell, they undergo an amplification process identical to that of a standard input pulse. So, to computationally validate our method for ASE output, we formed a prediction for the output at one end. Next, we formed a similar prediction to validate the model's calculation for ASE + ASE_r output. Finally, we collected data for various lengths, diameters, and initial gains to establish trends in the way ASE affects the population inversion. To validate our model on a broader scale, we compared our trends to those calculated with Equation 2.11.

3.2.1 Prediction Formulation. To form a prediction for the ASE output at one end we took advantage of the fact that each cell's contribution is the equivalent of an infinitesimal pulse. For example, a 30-centimeter cell in the middle of a one-meter amplifier would generate a photon density of 1.8×10^{10} during one time step if the initial gain coefficient was 50 percent per meter. $2\sigma\eta$ for this case is 5.5×10^{-13}, which is clearly less than the value for $\exp(-\Delta_0 \sigma L)$, 0.6. Thus, the criteria for an infinitesimal pulse is satisfied.

Because infinitesimal pulses are amplified according to the exponential law, our prediction is simple to formulate. First, we considered the forward traveling ASE in an

amplifier with zero reflectivity. If we let A, B, C, and D be the photon densities generated

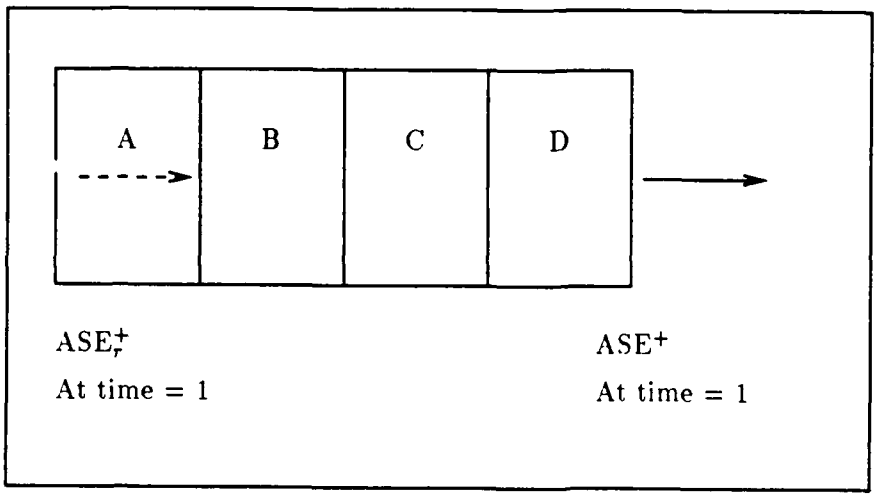

Figure 3.4. Amplifier cells modeled for ASE generation

by the four cells shown in Figure 3.4, the outputs for the first four time intervals are:

$$\text{ASE}out_1 = De^{gL} \tag{3.7}$$

$$\text{ASE}out_2 = (D + Ce^{gL})e^{gL} \tag{3.8}$$

$$\text{ASE}out_3 = (D + (C + Be^{gL})e^{gL})e^{gL} \tag{3.9}$$

$$\text{ASE}out_4 = (D + (C + (B + Ae^{gL})e^{gL})e^{gL})e^{gL} \tag{3.10}$$

where g is the gain coefficient and L is the length of a cell. At time step 4, all points in the amplifier are contributing to the ASE$^+$ output. Once we confirmed the model's ASE output at that end matched our prediction, we took our validation one step further by checking for similar output at the opposite end of the amplifier. With the amplifier divided into an even number of cells, the ASE$^-$ outputs balanced the ASE$^+$ outputs to five decimal places. If the time step used to divide the amplifier results in one cell being shorter than the others, a small deviation from symmetry occurs. These deviations were attributed to the values calculated for the solid angle, Ω, and are discussed further in Appendix D.

Theoretically, Equation 3.10 will describe the ASE output for all future time intervals.

Eventually though, the population of the excited state molecules will show noticeable decrease. This happens first in cell D. At this point, the values for g and A, B, C, D will decrease slightly and continue to decrease until the cell is saturated. All of these variables now have a spatial dependence based on the population of the excited state molecules. Figures 3.5 and 3.6 illustrate these concepts. Figure 3.5 shows the total ASE output over time. Starting at zero, it rises to a peak and then decreases as the gain falls off. Figure 3.6 shows the gain profile under the influence of ASE.

Of special note here are the conditions that were set up to show these dramatic ASE effects. The amplifier was relatively long (9 meters) and broad (10 centimeters). It also had a gain coefficient of over 200 percent per meter. These conditions are required for two reasons. Most importantly, the Einstein coefficient for spontaneous emission, A_{21}, is extremely small for the $J19 - J20$ transition of CO_2. Another reason is that we have assumed zero percent reflectivity.

3.3 Reflected ASE

As explained earlier, reflected ASE can lead to even more dramatic effects on the gain profile. Considering the amplifier cells in Figure 3.4 again, we can see that reflected ASE begins to play a major role after time unit four, when all cells are contributing reflected photons to the output. The equations for the next two time steps are:

$$\text{ASE}out_5 = R1 + (D + (C + (B + Ae^{gL})e^{gL})e^{gL})e^{gL} \tag{3.11}$$

$$\text{ASE}out_6 = R2 + (D + (C + (B + Ae^{gL})e^{gL})e^{gL})e^{gL} \tag{3.12}$$

where $R1$ is the amount of ASE reflected from the opposite end during the first time step and $R2$ is the ASE reflected during the second time step. The ASE outputs for subsequent time steps are calculated similarly. For this validation process, we considered each reflected term as an infinitesimal input pulse, so they could be calculated using:

$$R = \Re(\text{ASE}_r)e^{gL} \tag{3.13}$$

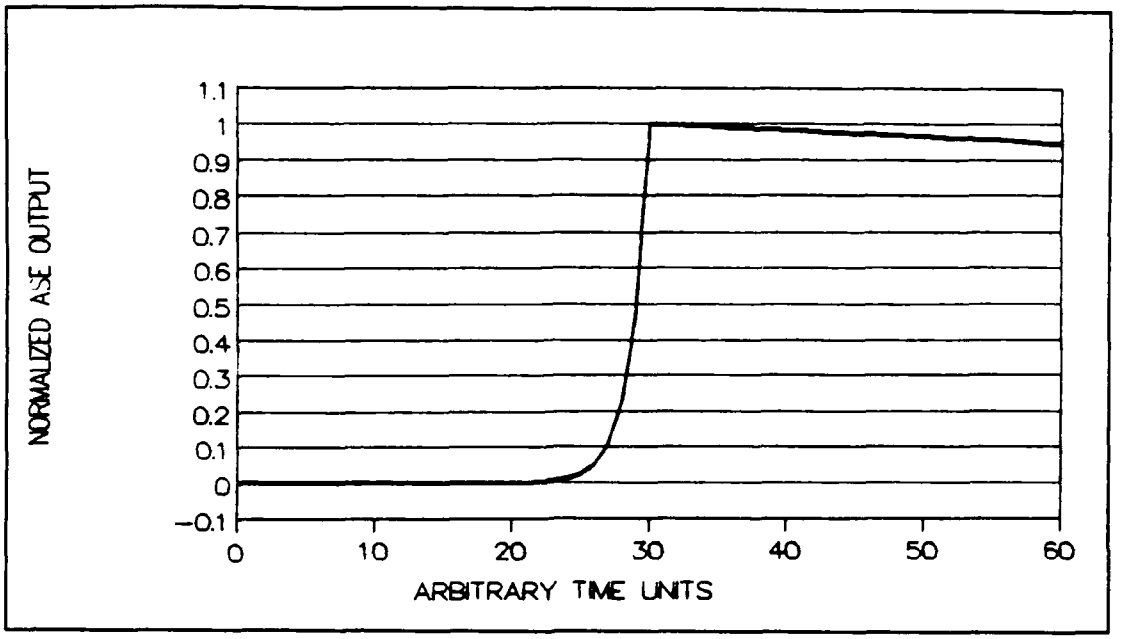

Figure 3.5. Total ASE output as a function of time

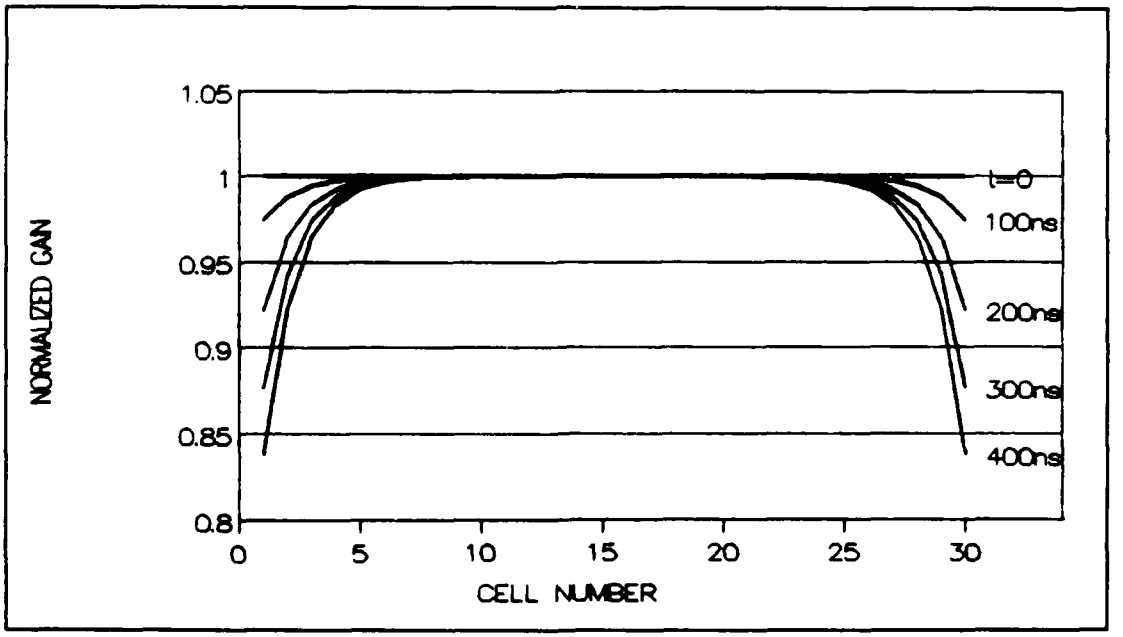

Figure 3.6. Gain profile under the influence of ASE

where ASE_r is the portion of ASE that will exit the opposite end of the amplifier, and L is the distance to that end. Using these equations to form a prediction, we validated our approach to calculating the growth of ASE with reflected contributions. Again, the outputs from both ends balanced each other.

Because $ASEout_2$ is greater than $ASEout_1$, $ASEout_6$ will be greater than $ASEout_5$. Logically, $ASEout_{n+1}$ will continue to be greater than $ASEout_n$ until the population inversion is sufficiently reduced. With a reflected contribution, the growth of ASE intensity resembles the growth of a pulse within an oscillator. The curves in Figures 3.7 and 3.8 demonstrate these characteristics. It is important to note that the data for these graphs came from runs using an amplifier with the same dimensions, but *half* the gain as in the previous set of graphs. Figure 3.7 shows an interesting growth pattern in the ASE output intensity. The surges in the curve represent cycles of amplification. The first surge is the growth prior to the exit of any reflected ASE. The next surge shows ASE that includes one reflection. Each of the following surges includes one more reflection. In this case, the gain is sufficiently reduced after only three reflections. Figure 3.8 shows that the depletion in the gain profile is not limited to the ends of the amplifier. The fact that these results came from an amplifier with half the initial gain emphasizes the significance of reflected ASE. As mentioned in the previous chapter, the most effective way to limit this gain reducing factor is to decrease the window reflectivity. Figure 3.9 displays the rate of gain reduction for various window reflectivities. Clearly, a good anti-reflective coating allows an input pulse to experience a higher gain profile for a longer period of time.

3.4 ASE Trend Comparison

To make our ASE validation more complete, we used the model to generate data on the same parameters used in Equation 2.11. In terms of length, diameter, and initial gain, Equation 2.11 describes how ASE can significantly limit amplifier design. To collect data in a consistent fashion, we defined three criteria for "significantly limited."

During the derivation of Equation 2.11, the sources did not indicate a consideration the time factor involved. Obviously, over an extended period of time, ASE would eventually saturate the entire amplifier. However, we are interested in a time period limited to

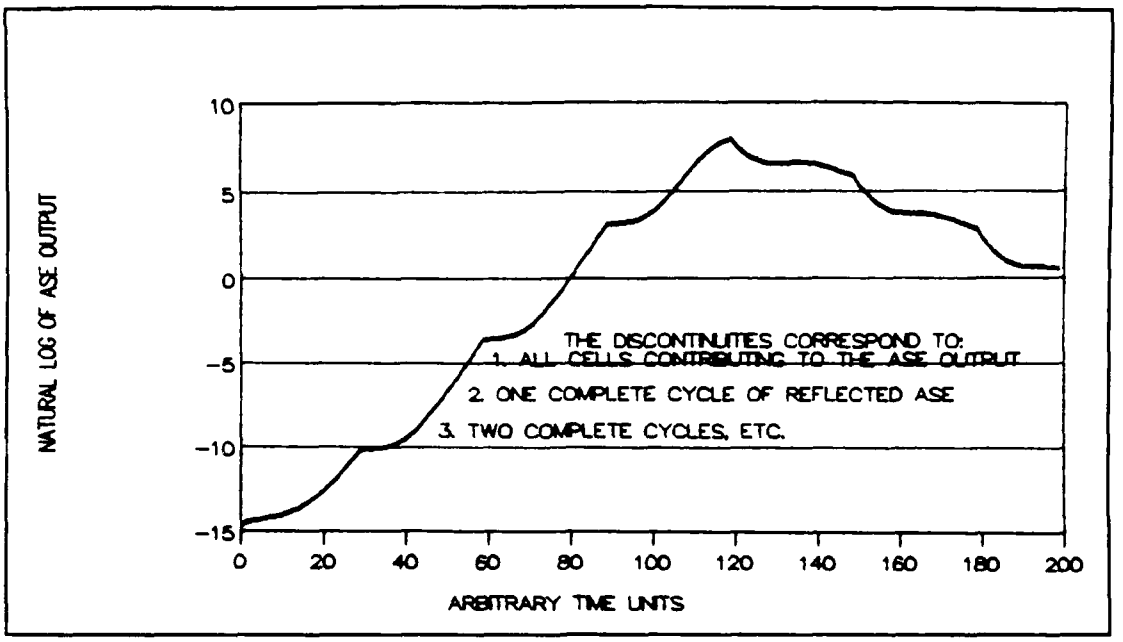

Figure 3.7. Total ASE output as a function of time with reflectivity consideration

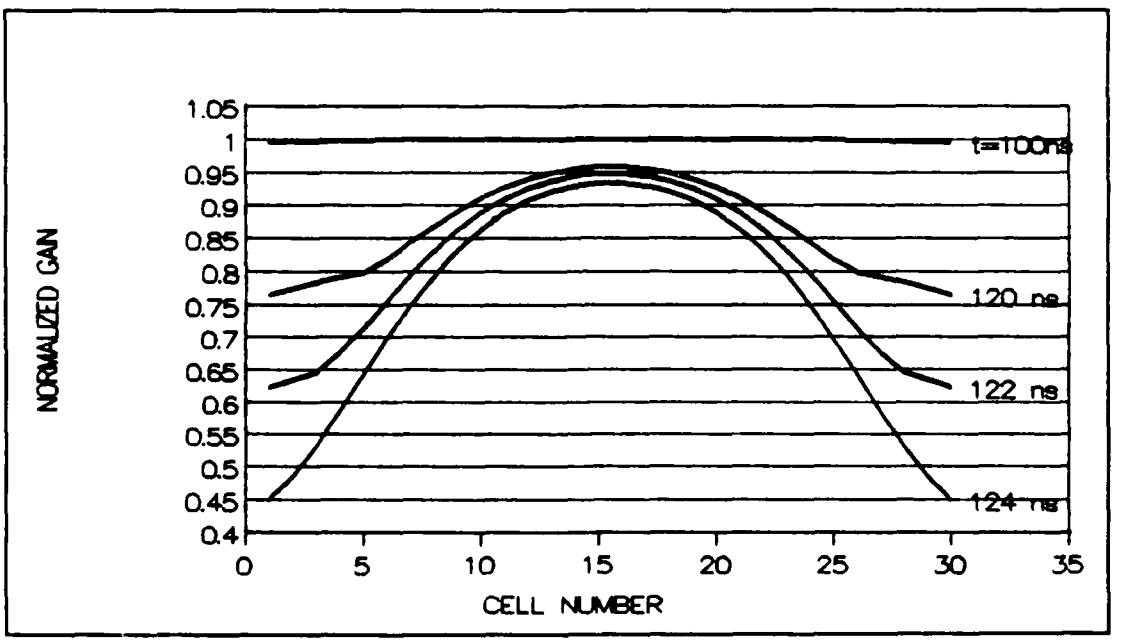

Figure 3.8. Gain profile under the influence of ASE and reflected ASE

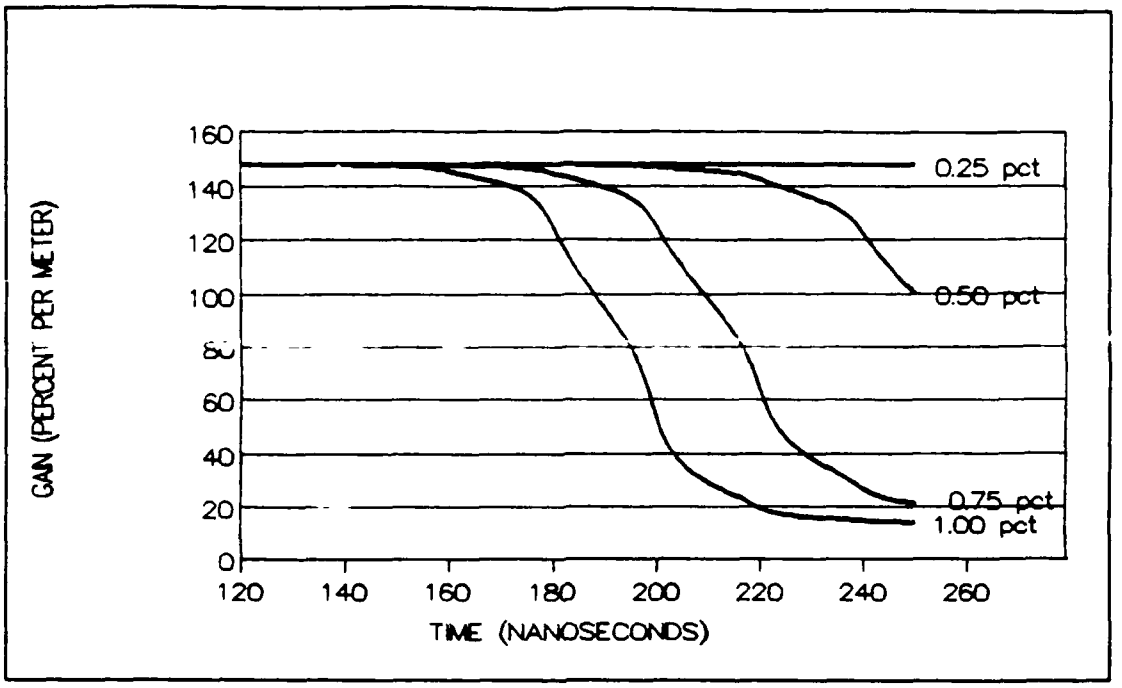

Figure 3.9. Rate of gain reduction as reflectivity increases

establishing a population inversion and delivering an input pulse to it. By approximating this period of interest as 200 nanoseconds, we define our first criterion.

Our second criterion locates our region of interest. Because ASE cripples an amplifier symmetrically from the ends toward the center, we monitored the gain drop-off in the first cell to detect the initial ASE effects. For convenience we set the length of the cell at 30 centimeters.

To be significantly limited, a portion of the amplifier does not have to have a gain coefficient of zero. For example, if the gain coefficient in a three-meter amplifier is 100 percent per meter, its small-signal gain is 20.08. For the same length amplifier and only 50 percent per meter, the small-signal gain is 4.48. Because reducing the gain coefficient by a factor of two has such a large effect, we used it as our last criterion.

Putting the criteria together, our data collection involved three steps. First, a length, diameter, and gain coefficient were selected. Second, we monitored the gain coefficient in the first cell for 200 nanoseconds. In the next step, the initial gain coefficient is adjusted, if

necessary, and steps one and two are repeated. The third step is accomplished if the gain coefficient does not drop to half its original value (±0.1%/meter) within 200 nanoseconds. Figure 3.10 shows how sensitive the rate of gain reduction is to changes in the initial gain coefficient. Our results appear in Table 3.2 and match the trends shown in Figure

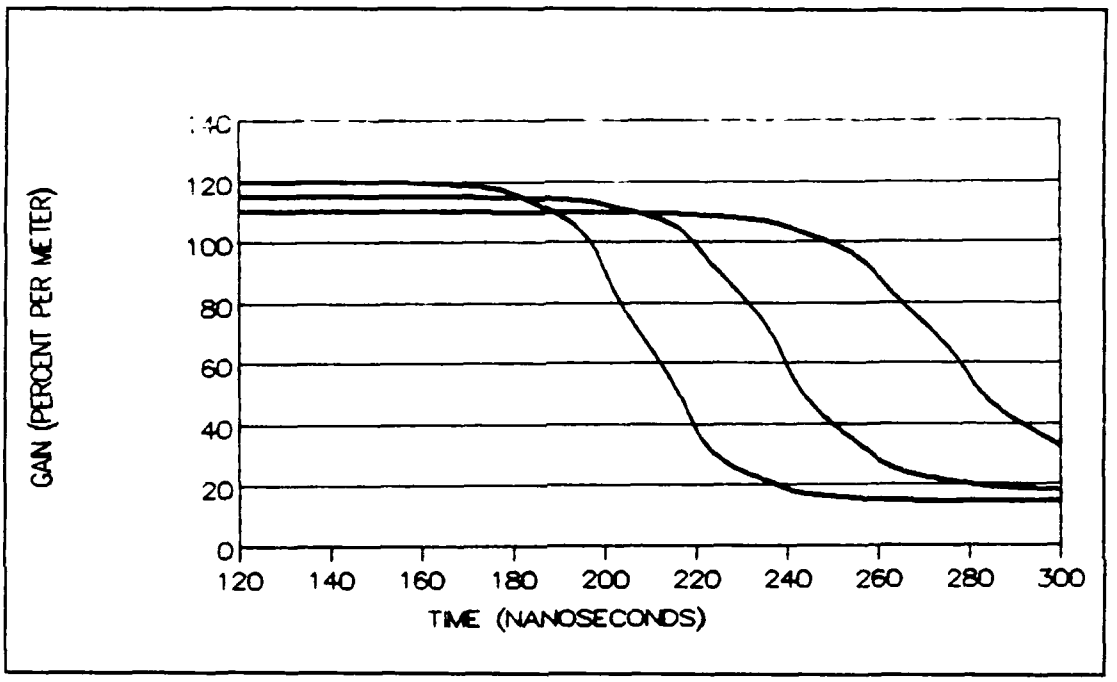

Figure 3.10. ASE effects on amplifier gain as a function of time and initial gain coefficient

2.10. These results and those calculated with Equation 2.11 are especially close for the sensitivity of ASE intensity to length. However, for shorter amplifiers, the model's results do not show as much sensitivity to changes in the diameter. One explanation for this is our large cell size. With a large cell size, we do not consider the large increase in solid angle for positions close to the amplifier ends.

3.5 Reflected Input Pulse

The reflection of the input pulse is another factor that can reduce the gain inside the amplifier. Because similar processes had already been validated, the validation of this factor was more of a verification. To accomplish the "validation" of this factor, we created

Table 3.2. Parameter combinations satisfying the three ASE significance criteria in section 3.4

INITIAL GAIN COEFFICIENT %/meter			
DIAMETER (meters)	LENGTH = 2m	LENGTH = 6m	LENGTH = 10m
0.02	313.60	126.61	96.36
0.04	311.30	124.00	93.88
0.06	310.00	122.48	92.41
0.08	309.20	121.40	91.37
0.10	308.50	120.56	90.57
0.12	308.10	119.87	89.91
0.14	307.75	119.28	89.35
0.16	307.45	118.77	88.87
0.18	307.20	118.33	88.43
0.20	306.90	117.95	88.06
0.22	306.70	117.59	87.71

a pulse with a duration equal to our cell length divided by the speed of light. Such a pulse "fits" exactly into only one cell. Then we simply observed its amplification and reflection. Next, we monitored the reflection's effect on the population inversion in each cell as it traveled back and forth. These effects were verified with hand calculations.

The only inaccuracy we found dealt with the timing of the reflection in cases where the length of the amplifier was not divided into an even number of cells. Regardless of the length of the last cell, the reflection required one full time step to reenter it. For very short "fractional" cells, the error is maximized. In effect, the reduction in gain by the reflected input pulse is delayed by nearly a full time step. After examining the output pulses from amplifiers with and without "fractional" cells, we determined that this error was insignificant.

3.6 Summary

Through a series of verifications and comparisons, we have demonstrated the validity of our model. Most importantly, in the calculation of the spatial and temporal dependence of the amplification process, the model's results agree with those calculated with an an-

alytical solution. In this chapter, we showed that this agreement held for inputs ranging from infinitesimal pulses to large pulses capable of saturating the entire amplifier. Once this process was validated for a single pass in the forward direction, we used it to calculate the bi-directional amplification of ASE, reflected ASE, and a reflected input pulse.

Treating each cell as an input source, ASE output was calculated as a sum of exponential growths. Using similar equations for backward traveling ASE, symmetric results were obtained, thus validating amplification in both directions. The most interesting ASE results involved multiple reflections between the cavity windows. To model this effect, the only change made to the existing model was to calculate the fraction of ASE that could be reflected and still contribute to the ASE output. We estimated this fraction using a conservative approximation for ASE's angle of divergence. Again, the outputs from both ends of the amplifier were symmetric in both time and amplitude. We verified our model further by comparing its parameterized results with an analytic equation.

IV. Results

Thus far, all of our results have been based on amplifier operation involving an instantaneous population inversion. In the absence of an electric pump and gas kinetics, the only influences on the population inversion have been spontaneous and stimulated emissions. Since the kinetics and pumping portions of Stone's oscillator model have already been incorporated into this model, we can calculate results based on all four gain factors. Rather than assuming these results will be valid, we performed several tests to confirm the soundness of our comprehensive model.

Two sets of tests were performed. In the first set, we dealt with helping the user determine how small the time step should be to achieve accurate results. This model does not use a variable time step algorithm to do its numerical integrations. Such an algorithm would automatically find a time step for a selected accuracy. For example, the user might input a maximum allowable change in a cell's gain and the algorithm would iterate until it finds an appropriate time step. Because the time step determines the number of cells, each new time step attempted would create a new set of amplifier divisions and require the program to restart. For this reason, the variable time step algorithm was not used and this first set of tests was performed. The second set of tests involved a few excursions into the vast array of possible parameter combinations. Specifically, we compared amplifications involving the following parameters:

1. ^{12}C and ^{13}C isotopes.
2. Temperature, holding number density constant.
3. Long, high-gain amplifiers with ASE consideration.

4.1 Determining a Practical Time Step

In general, numeric solutions provide better accuracy with smaller time steps. For our model, smaller time steps mean more amplifier divisions. Because gas kinetics is involved in determining the gain profile, the leading edge of the pulse will no longer experience constant gain. For this reason, the amplifier must be modeled with many cells even if the

pulse has a very short duration. In the model, the number of cells is a function of amplifier length and time step.

To relate time step to accuracy, we started with a large time step and monitored the propagation of three short pulses through a three-meter amplifier. The intensities of the inputs were 1, 2, and 4 MW/cm^2. In subsequent runs for each input we reduced the time step until the value for the output intensity converged. Table 4.1 shows the amplifier divisions and output change obtained using various time step values. Figure 4.1 shows the output convergence resulting from these time steps. As shown in Table 4.1, the net

Table 4.1. Percent change in output intensity

Cells	Time Step (ns)	Output Change (%)
1	10.00	—
2	5.00	+ 10.16
3	3.33	+ 3.51
4	2.50	+ 1.76
5	2.00	+ 1.06
6	1.67	+ 0.71
7	1.43	+ 0.51
8	1.25	+ 0.37
9	1.11	+ 0.30
10	1.00	+ 0.23

change in the output intensity was always positive. The reason the output values keep increasing is that each additional cell allows one more iteration of gain calculations before the pulse reaches the end of the amplifier. During this time interval, the pump is off, but there is still a large population of excited nitrogen molecules. These molecules collide with CO_2 molecules, transfering more of them into the $v = 001$ energy level, and consequently, increasing the gain. As a result, the pulse is amplified to a steadily higher value. For each time step change, all three input intensities had the same percent change in their output intensity. These changes ranged from over 10% to less than 0.25%. If the amplifier length was doubled, these changes were also doubled. Using a time step of one nanosecond, we were able limit these increases to under one percent—even for an amplifier 12 meters long. These small changes indicate that, for this time scale, typical gas kinetic rates cause

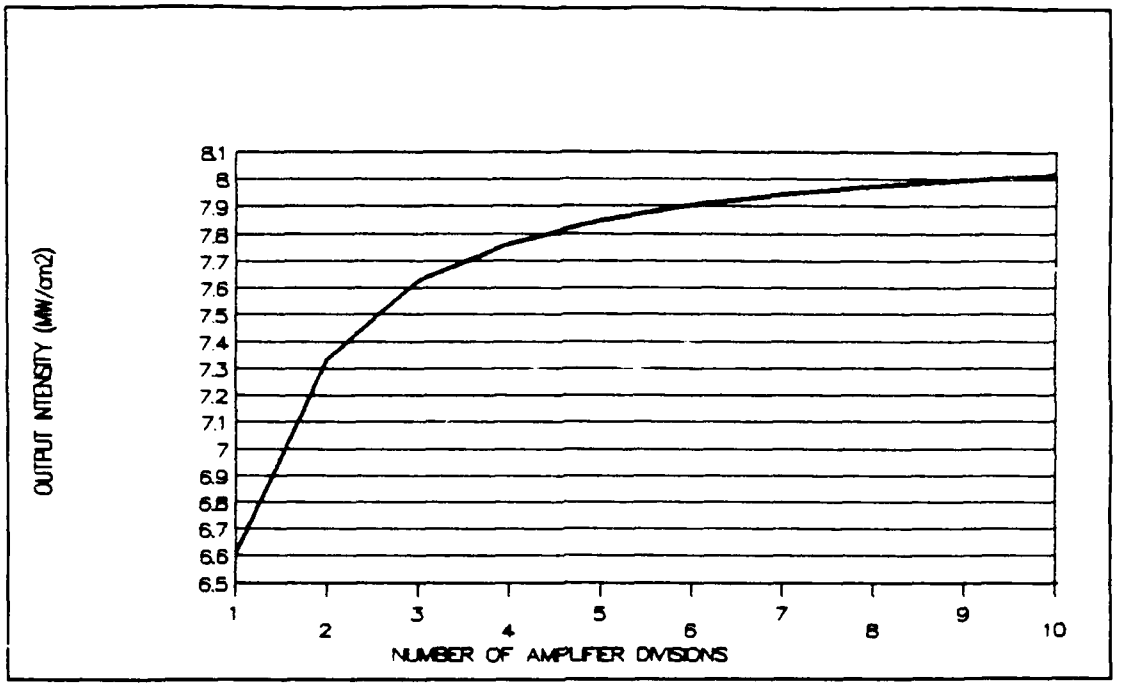

Figure 4.1. Peak pulse output as a function of time step

insignificant changes in the population inversion.[1]

In addition to analyzing the percent change in the output intensity for each time step, we also looked at the maximum reduction in the last cell's gain during one time step. As the time step was reduced, the gain reduction became less severe. Furthermore, for each time step, the percent change in the maximum gain reduction was the same for all three input intensities.

Another consistency found in this test was the relative error between the peak power calculated with these time steps and the peak power calculated using the maximum number of amplifier divisions. The maximum number of divisions was determined by computer memory limits. For input intensities of 1, 2, and 4 MW/cm^2, we found the relative error at each time step to be identical. This error also dropped to less than one percent when the number of amplifier divisions was increased to eight and continued to drop as the number

[1]The population inversion is essentially frozen for these small time steps only because we have assumed equilibrium among the rotational levels.

of cells increased.

All of these consistencies encouraged us to find a relationship that would use the peak power and the maximum gain change to determine an indicator of relative error. Such an indicator would tell a user when he was "close enough" and avoid extra time-consuming runs with smaller time steps. After examining several amplifier lengths and gain profiles, we found that an expression for an error indicator involved more terms than previously anticipated. A ratio combining peak power, cell length, and maximum gain reduction produced promising results for limited cases. However, for longer, higher gain amplifiers this ratio generated nothing resembling a numerical trend.

So, to aid the user in selecting an appropriate time step, our only conclusion is that a time step of one nanosecond will allow the model to keep up with the changes in the gain profile due to gas kinetics. We saw in the validation section that this time step allows the model to generate pulse shapes within one percent of Frantz and Nodvik's closed-form solution for many combinations of amplifier length, gain, and input intensity. However, extreme values of those parameters will require smaller time steps to control the error induced by rapid gain reduction.

4.2 Amplification Using ^{12}C and ^{13}C

To begin our second set of confirmation tests, we compared the amplification of identical inputs using two different gas mixes. The first used ^{12}C and the second used ^{13}C. The kinetic rates for the two mixes were very similar. So, for our calculations, the only significant differences between the them were their line center frequencies (2.83062×10^{13} Hz for ^{12}C and 2.68887×10^{13} Hz for ^{13}C) and their values for A_{21} (0.194 for ^{12}C and 0.208 for ^{13}C). Because the stimulated emission cross section is inversely proportional to line center frequency squared, and directly proportional to A_{21}, we expected the gain profile to be higher for ^{13}C. Figure 4.2 compares the outputs from two amplifier lengths for both isotopes. The ^{13}C output values have been normalized to one for both cases. In general, the longer the amplifier, the greater the difference between the peak power outputs. This result shows that in addition to having better transmission through the atmosphere, a laser using ^{13}C also has higher amplification efficiency.

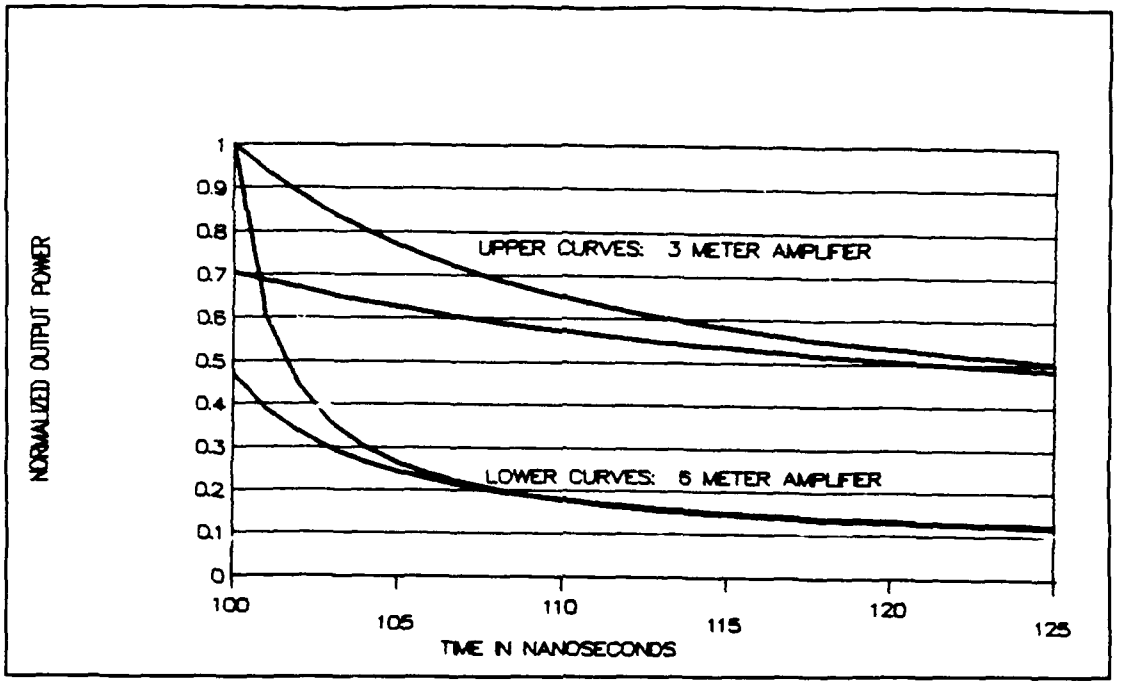

Figure 4.2. Relative output intensities for ^{12}C and ^{13}C (^{13}C normalized to 1 for both cases)

4.3 Temperature Dependence

In this test, we wanted to check the effect temperature had on the amplifier gain profile and the resulting pulse amplification. To isolate this effect, we controlled the number density of the gases by keeping the pressure-to-temperature ratio constant. Temperature was varied from 250 K to 500 K. Raising temperature and pressure results in higher collisional relaxation rates. The symbols for the relaxation rates of the upper and lower laser levels are γ_A and γ_B, respectively. γ_C is the symbol for the collisional rate at which energy is transferred between the excited states of nitrogen and CO_2. These relationships are illustrated in Figure 4.3. Increasing the temperature and pressure also results in a lower value for the stimulated emission cross section (σ).[2] Table 4.2 displays the values for these terms for each temperature. The value of σ is reduced as the temperature rises

[2] As mentioned earlier, only the initial values of these terms are modeled to be temperature dependent. Since temperature increases during amplifier operation, our modeled effects will not be as dramatic as the actual effects.

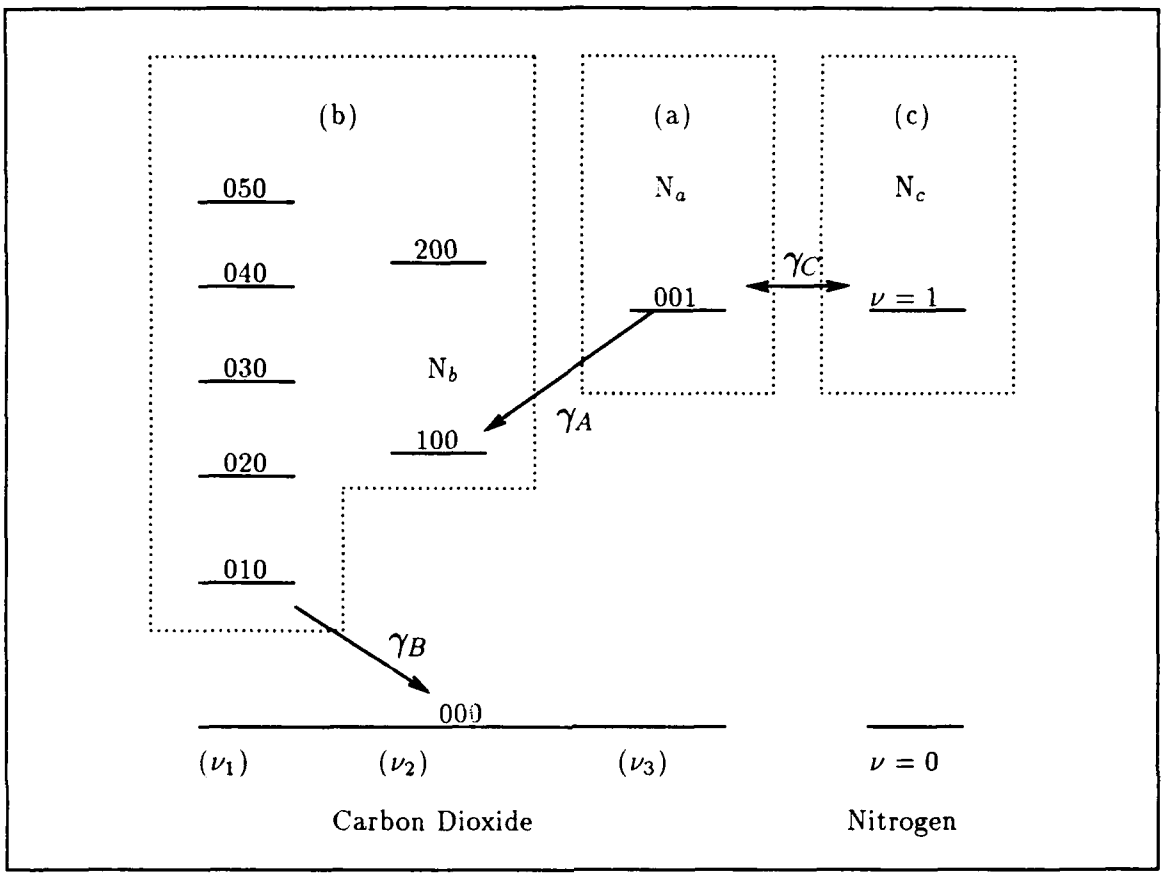

Figure 4.3. Diagram of the kinetic relationships in a four-level CO_2 laser model

for two reasons. First, $F_{u(J=19)}$ decreases with increasing temperature and, second, $\Delta\nu_p$ increases. Because σ gets smaller, the initial gain in the amplifier falls off.

The data in Table 4.2 was calculated using Melançon's temperature model and shows that temperature most significantly affects γ_B.(13) As a result, the population inversion increases faster for higher temperatures. The increasing slopes of the gain curves in Figures 4.4 and 4.5 illustrate this effect. It is also evident in Figure reffigure29a that even though the initial slope of the gain curve is steeper for higher temperature, the curve peaks out earlier. The data in Table 4.2 indicates that this effect is due to the changes in the kinetic rates that affect the upper lasing level, γ_A and γ_C. Increasing temperature increases both rates. However, over the temperature range, γ_A changes by a factor of 9, while γ_C changes by a factor of about 5.7. Thus, the population inversion grows at a progressively

Table 4.2. Parameters affected during the temperature dependence test

Temp (K)	$\gamma_A(s^{-1})$	$\gamma_B(s^{-1})$	$\gamma_{C_{CO2}}(s^{-1})$	$\gamma_{C_{N2}}(s^{-1},$	$\sigma(m^2)$	$GAIN_0(\%/m)$
250	.0005	.0098	.0100	.0110	9.50 E-24	-01.11
300	.0010	.0246	.0158	.0174	8.32 E-24	-03.54
350	.0017	.0492	.0233	.0256	7.31 E-24	-07.79
400	.0025	.0849	.0325	.0358	6.45 E-24	-13.62
450	.0035	.1325	.0437	.0480	5.73 E-24	-20.51
500	.0046	.1924	.0568	.0625	5.13 E-24	-27.84

slower rate.

The data has been displayed on two graphs for two separate comparisons, one between the effects o' temperature on gain development, the other between the gain depletion at the beginning and the end of the amplifier. It should be kept in mind that prior to the arrival of the input pulse (t = 330 ns) the gain profile is uniform across the amplifier. In the first comparison, we noted that increasing kinetic rates lead to faster gain development, including earlier level-off. Higher kinetic rates also result in quicker recovery of the gain after the pulse has passed through the amplifier. The second comparison simply illustrates the severity of the gain depletion in the last cell.

The output pulses for the first three temperatures are shown in Figure 4.6. Despite starting at smaller gain levels, higher temperatures produced significantly higher gain profiles. Thus, the output pulses had higher peaks for higher temperatures. There were also indications of more pulse narrowing. For higher temperatures, the peaks occurred earlier in time and the pulse width between the half-max points was narrower.

However, for temperatures beyond 400 K, these trends were reversed. As shown in Figure 4.7 the pulses had lower peaks, the peaks occurred later in time, and the pulses grew wider rather than narrower. Beyond 400 K, the gain leveled off at progressively lower levels, resulting in less rapid pulse growth and a lower peak. Because the pulse grew less rapidly, the rate of change in gain was smaller. Higher kinetic rates, forcing a higher population inversion, also caused the gain to drop off more slowly. With higher gain for

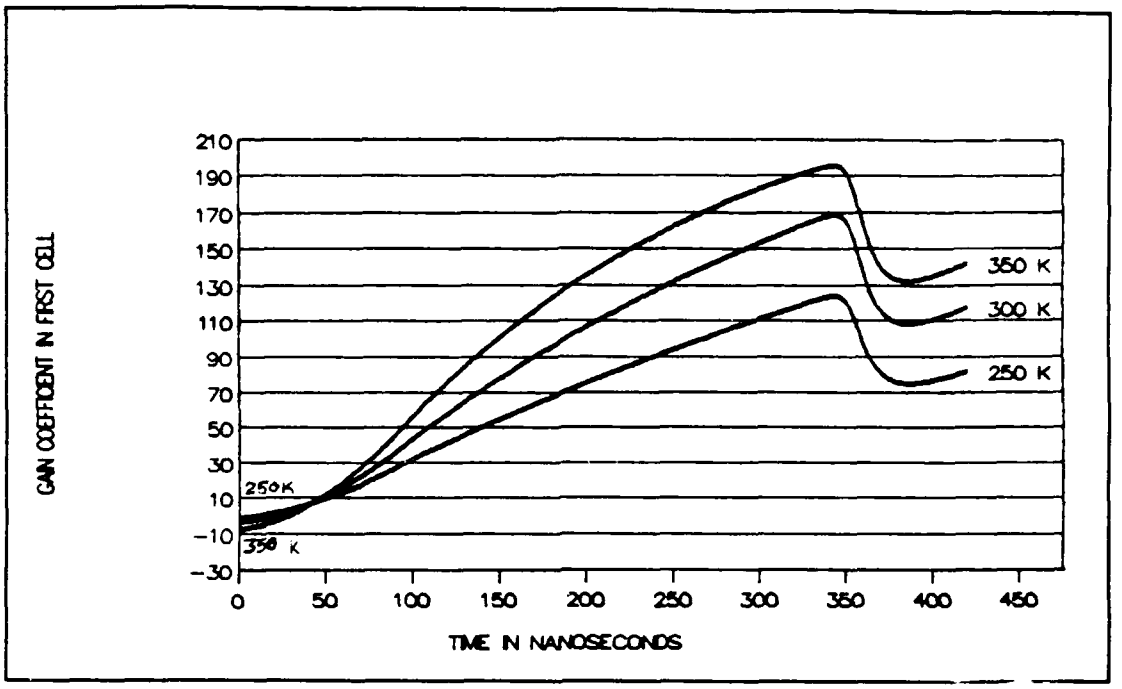

Figure 4.4. Gain as a function of time and temperature (first cell)

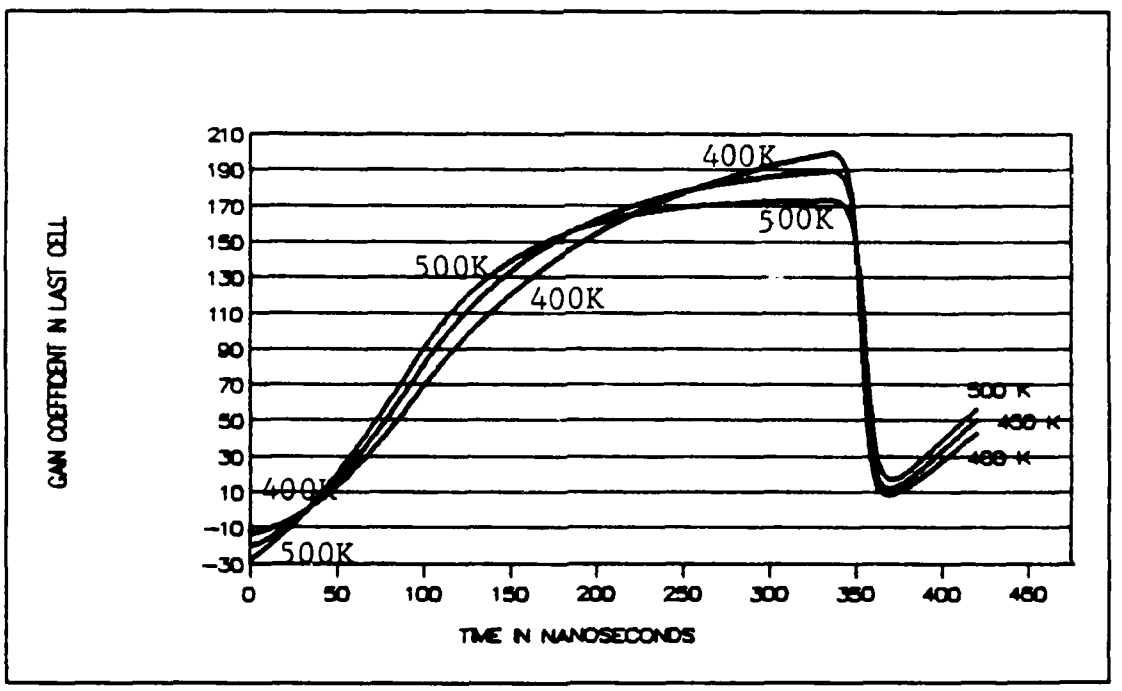

Figure 4.5. Gain as a function of time and temperature (last cell)

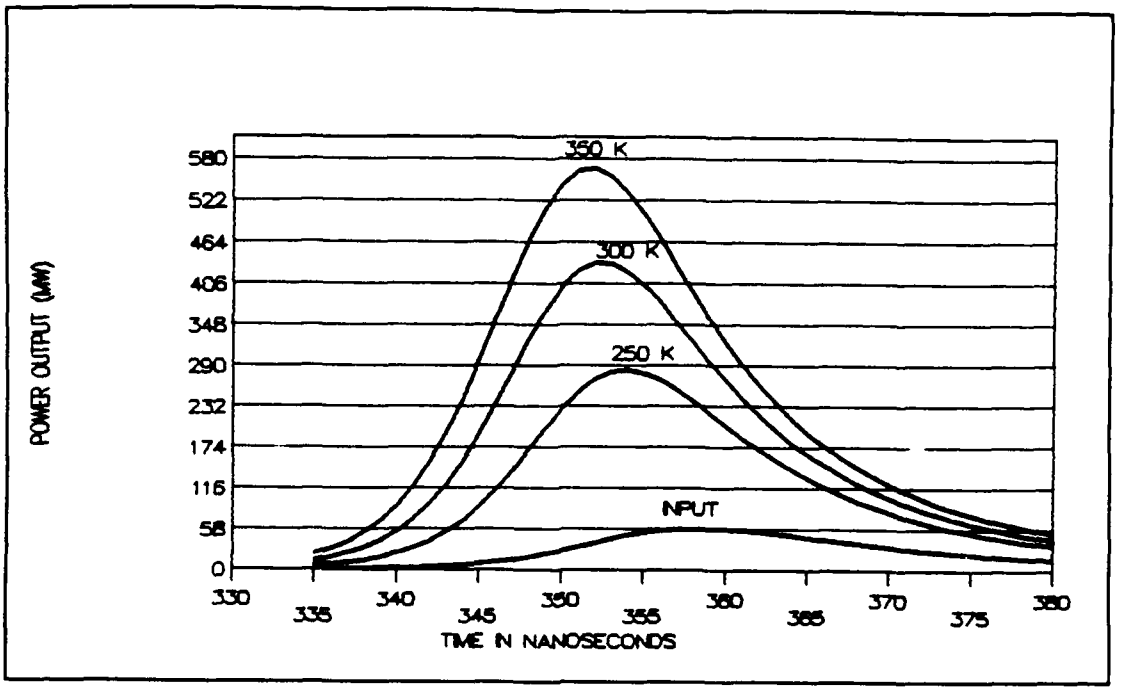

Figure 4.6. Output pulse narrowing for increasing temperatures

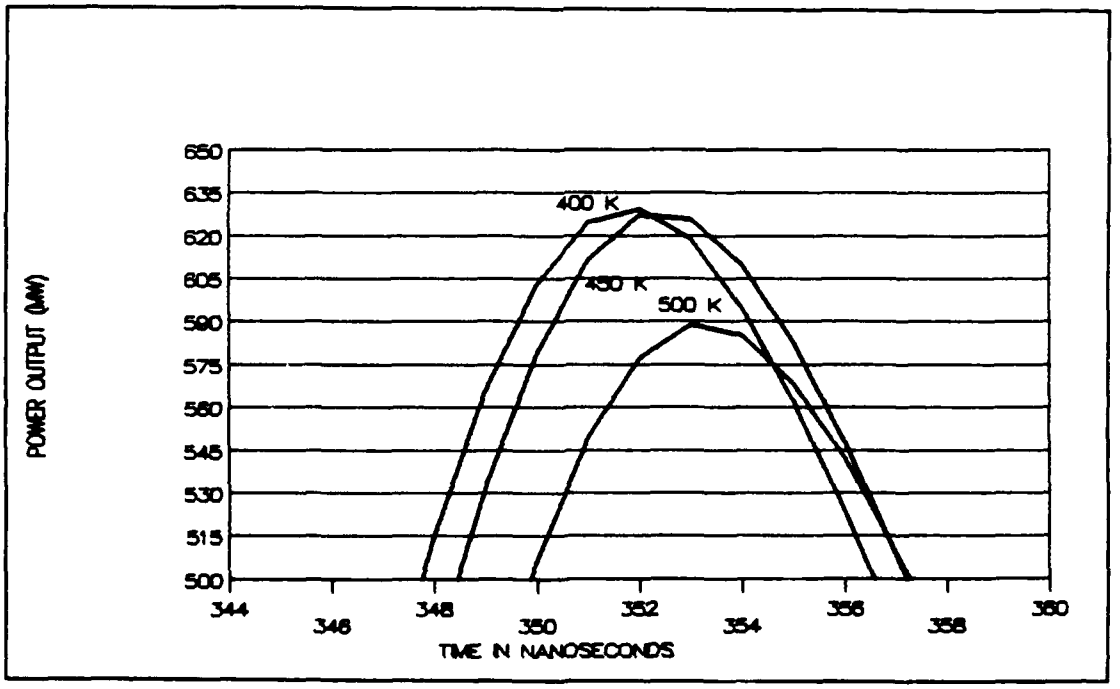

Figure 4.7. Output power peaks for increasing temperature

later segments of the input pulse, the output pulse was broader and had a peak that was moved forward in time.

4.4 Amplification with ASE Effects

The last test in this chapter examined the effects of ASE in the presence of gas kinetics. From previous analysis, we knew that ASE effects were noticeable in long, wide amplifiers with relatively high gain profiles. Also, it takes over 150 nanoseconds for both the population inversion and the ASE intensity to grow to desired levels. So, to evaluate the effects of ASE, we used an eight-meter amplifier with a diameter of five centimeters. The gas mix used was a 10:10:80 mix of CO_2, N_2, and He at 300 K and one atmosphere of pressure. Also, the pump duration was fixed at 100 nanoseconds. With this set-up we performed three model runs.

In our first run, we used windows without anti-reflective coating and a very high pump efficiency (40%).[3] For the second run, we reduced the reflectivity of the windows from 4% down to 1% and performed runs with pump efficiencies of 25, 30, and 35 percent. Leaving the pump efficiency at 35%, in our third run, we varied the reflectivity of the windows from 1% down to 0.01%.

Though the gas mix and the amplifier diameter were fairly standard, our first run showed that ASE could significantly affect the gain profile in less than 200 nanoseconds. Figure 4.8 shows that the ASE output and its effect on amplifier gain are very similar to the operation of a gain-switched oscillator. Looking at the tail of the ASE pulse, we found that our results concurred with Vereyen's conclusion that once ASE reaches saturation intensity, "further pumping of the amplifier is futile; spontaneous emission extracts the energy from the inversion as fast as the pumping agent can create it" (24:183).

In the second run, we found that despite reducing the reflectivity from four percent down to one percent, ASE was still able to saturate the amplifier. Figures 4.9 and 4.10 show that lowering the pump efficiency will delay the saturation and slightly reduce the magnitude of the ASE output pulse.

[3]In our model, pump efficiency refers to the percent of N_2 molecules that will transition to the $v = 1$ excited state.

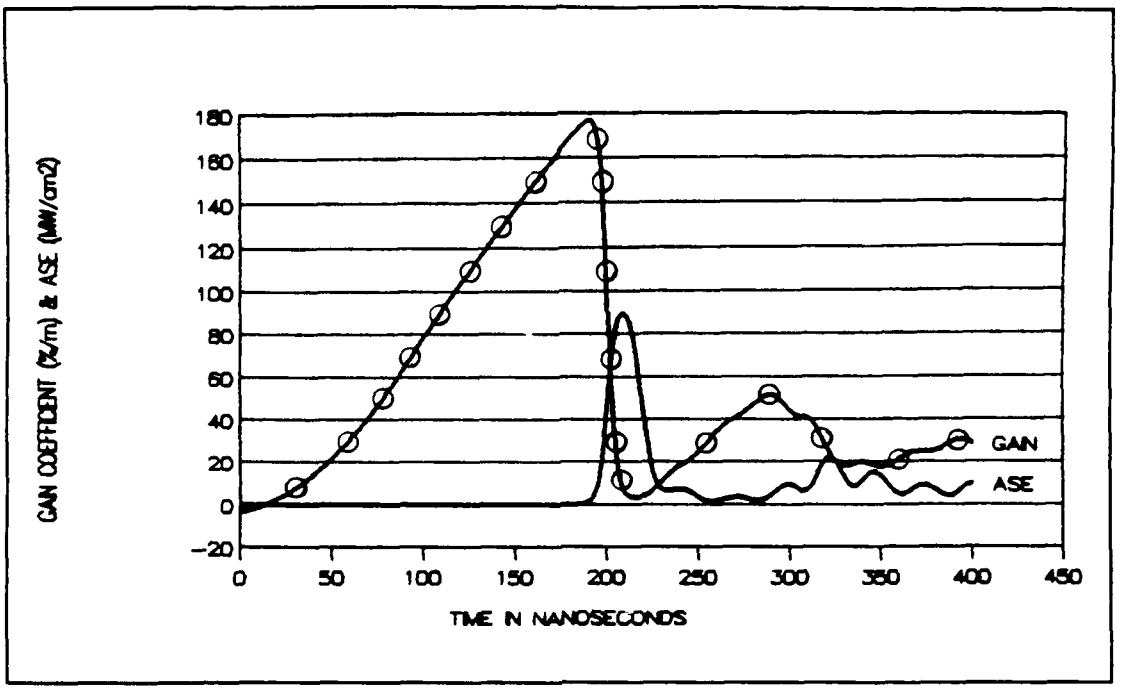

Figure 4.8. Gain evolution and ASE output as functions of time

In the third run, we found that reducing the reflectivity has results similar to reducing the pump efficiency. Figure 4.11 shows that output pulse is delayed more and more as the reflectivity is reduced. In addition, the magnitude of the output pulse intensity falls off for smaller reflectivities.

Although our approximation for ASE output is conservative, these examples illustrate the limitations ASE imposes on amplifier designs. All of these examples have indicated that for efficient amplification, an input pulse must enter the amplifier before ASE reaches saturation intensity. This timing is made easier if the window reflectivity is reduced and amplifier gain is limited. The amplifier gain can be limited by reducing the pump intensity, altering the gas mix, or coordinated timing of the oscillator and amplifier pumps. To allow this timing, our model allows the amplifier pump to be delayed relative to the oscillator pump.

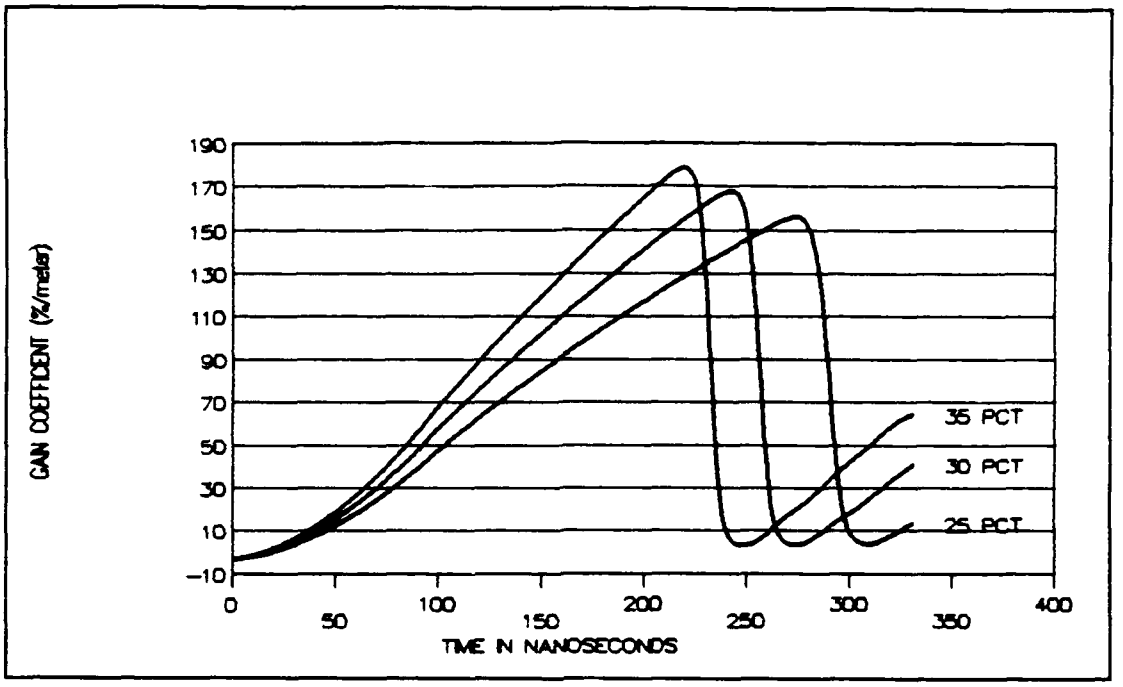

Figure 4.9. Gain as a function of time and pump efficiency under the influence of ASE

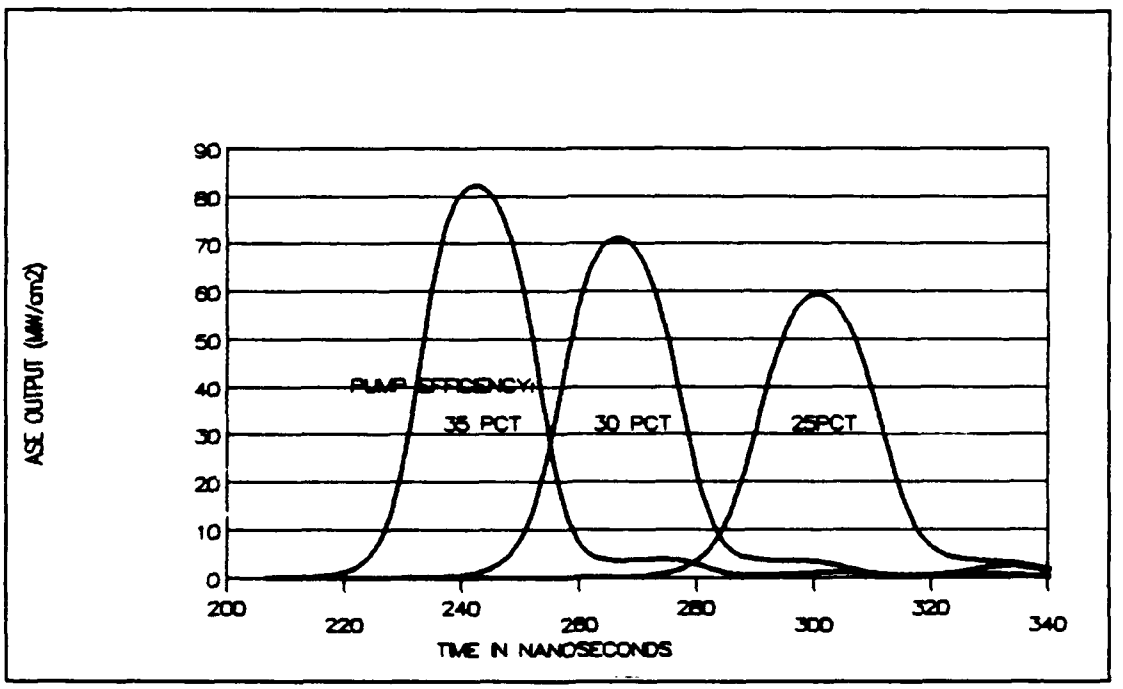

Figure 4.10. ASE outputs for various pump efficiencies

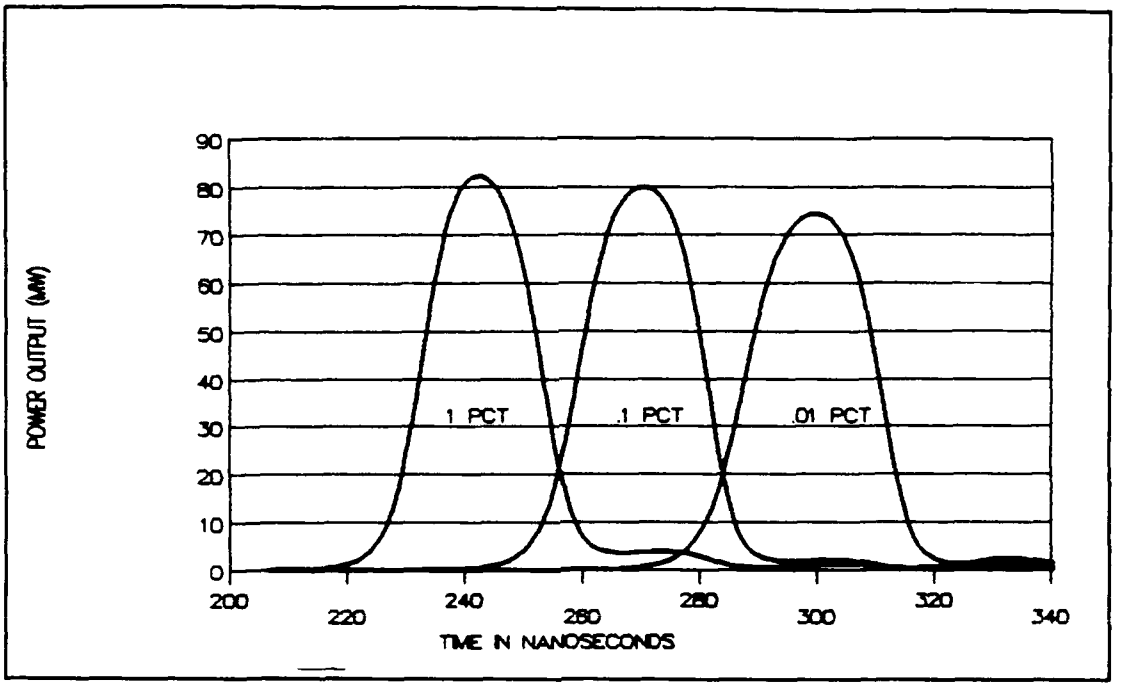

Figure 4.11. ASE outputs for various window reflectivities

4.5 Summary

In this chapter we have examined many aspects of our amplifier model to confirm the soundness of the combination of this amplifier model with a validated gas kinetics model. We established that because gain changes due to gas kinetics will be small, a time step of one nanosecond will be a good starting point for any amplifier analysis. Smaller time steps will be required when other factors result in large rates of gain reduction. These factors include amplifier length, gain, and input intensity. The next two tests analyzed the isotope and temperature parameters. The results were consistent with prediction. Finally, in the last section, we verified that the model had consistent results for ASE output involving gain profiles established by pumping and gas kinetics. Though it is not widely discussed in the literature, it appears that ASE is an important design consideration for large CO_2 amplifiers even though the A_{21} value for CO_2 is very small.

V. Conclusions and Recommendations

We have developed and validated a computer simulation of a CO_2 laser amplifier for use on IBM-compatible personal computers. It allows the input of square pulses as well as pulses generated with a typical laser oscillator. The other input variables are listed below:

1. Length and aperture diameter.
2. Gas mix formed with N_2, He, H, H_2O, and either $^{12}CO_2$ or $^{13}CO_2$.
3. Gas pressure and initial temperature.
4. Pump pulse shape, duration, and efficiency.
5. Time step/amplifier divisions.
6. Loss terms for absorption and window transmissivity.

The user can also choose to model amplification with or without gas kinetics and with or without ASE consideration. The ability to run the model without the last two parameters has been added for instructional purposes rather than for actual amplifier design.

The model's accuracy depends on the rate at which the gain is reduced from one time step to the next as the pulse propagates through any section of the amplifier. Higher rates of gain reduction are caused by higher pulse intensities and characteristically occur at the end of the amplifier. These higher rates result in larger errors in pulse shape and energy gain. Kinetics also play a role in changing the gain, but we have found that using one nanosecond time steps virtually eliminates this factor as a potential error source. Error trends for increases in pulse intensity, amplifier length, and amplifier gain were discussed in Chapter 3 and displayed in Figure 3.2. When using Figure 3.2 as a guideline, one should keep in mind that these are maximized errors for overall energy gain, and that pulse shape errors will be significantly smaller.

Several improvements to the model are possible and recommended for follow-on research. We will discuss four possibilities here. First, to improve the accuracy and extend the analysis capability, the model should be coded for use on a mainframe computer. This will allow time steps much shorter than one nanosecond and hundreds rather than tens

of amplifier divisions. Until a version is available on a mainframe, long amplifiers may be modeled using the detailed method described at the end of Appendix A. The second recommendation is to model the relaxation of the rotational levels as well as the vibrational levels. The third improvement does not necessarily require a mainframe for application. This improvement would be to increase the amplifier efficiency by allowing one of the windows to be totally reflecting and create a double-pass amplifier. Lastly, we recommend further work in the modeling of ASE. The ASE model requires a better approximation for the amplification of the entire band of ASE frequencies. Also, the results should be compared with experimental results for validation and error assessment.

Appendix A. *Notes to User*

This appendix outlines the use of this CO_2 amplifier model. It is divided into six sections. The first section provides general guidance and should be read before actually running the program. The following four sections describe the "filed-pulse" routine, the "square-pulse" routine, the output displays, and creating output data files. In the last section, we examine a method that can be used to circumvent the constraints imposed by the limited memory of personal computers.

A.1 General Guidance

To achieve reasonable results, the user should keep several things in mind. In this section, time constraints, memory constraints, and parameter limits will be discussed.

A.1.1 Time Step Effect on Run Time and Memory Limits. Smaller time steps lead to smaller relative errors. However, small time steps lead to longer run times and may cause the memory limit to be exceeded. Smaller time steps cause longer run times for two reasons, both of which are related to the number of integrations that will be done during the simulation run. First, a smaller time step breaks the period of interest into more time increments. Second, it divides the amplifier into more cells. One integration is done per cell per time increment, so the number of integrations for a given time step and amplifier length is given by

$$\text{Integrations} = (\text{tmax})/(\text{h1}) \times (\text{Length})/(\text{h1} \times \text{tcav} \times \text{c}) \qquad \text{(A.1)}$$

where tcav is the base time unit, tmax is the period of interest in base time units, h1 is the time step (fraction of the base time unit), and cLight is the speed of light. Sample integration values appear in Table A.1. Notice that when the time step is cut in half, the number of cells doubles, but the number of integrations quadruples. The time steps used to divide the amplifier into an even number of cells were calculated as follows:

$$\text{h1} = (\text{length})/(\text{tcav})(\text{c})(\text{number of cells}) \qquad \text{(A.2)}$$

Table A.1. *Influence of time step on the number of program integrations.* Length = 2 meters, tcav = 10 nanoseconds, tmax = 20

time step	Cells	Integrations
.1334	5	750
.1112	6	1080
.0953	7	1470
.0834	8	1920
.0741	9	2430
.0667	10	3000
.0606	11	3630

After each time step change, the number of integrations to be done is recalculated and displayed on the input screen. The user should keep in mind that the model executes approximately 3200 integrations per minute.[1]

For each integration, seventeen different variables are stored in memory for intermediate calculations and output displays. Since the amount of memory available is related to the number of integrations, it is also affected by time step reductions. Another reason memory available is sensitive to time step changes, is that eleven of the seventeen variables stored in memory are stored in two-dimensional arrays. After each change is made to the time step, the amplifier length, or the maximum run time, the program will display the user's available memory.

The factors that require the use of small step sizes and large volumes of memory also lead to high output intensity. For sound results, small time steps are required to describe amplification in the presence of any of the following: a long amplifier (L > 5 meters), a large input intensity (I > 5 MW/cm^2, or a high gain amplifier (g > 150 percent/meter). Guidelines for time step selection are as follows. (1) Start with a time step of one nanosecond. This value will keep up with any changes in gain due to gas kinetics. (2) The maximum gain change in the last cell will be displayed on the output screen following each run. As this value is minimized, so is the relative error. (3) While an

[1]This speed is an averaged value using a computer with an 80287-10 math coprocessor.

input pulse is propagating, if the gain coefficient in the last cell falls to a value less than the "loss-per-unit-length" term (α), then a smaller time step is recommended.

A.1.2 Parameter Limits. The following parameter limits are estimates. They are provided to help the user obtain accurate and valid results from this amplifier model.

Gas Mix The gas percentages should add up to 100 percent and there must be some percentage of CO_2. In the filed-pulse routine, the CO_2 isotope will be the same as the one used to generate the file during the oscillator run. Mixing isotopes between the oscillator and the amplifier would result in no amplification whatsoever.

Temperature The temperature-dependent collisional relaxation rates in this model are valid for temperatures > 200 K.

Pressure The model is valid only for pressures where the lineshape is Lorentzian. So, the pressure should be greater than 0.015 atmospheres.

Pump Efficiency Reasonable pump efficiencies include values up to 20 percent.

Loss Per Unit Length (α) Values for α vary with the gas mix and typically range between 2 and 4 percent.

Reflectivity Values for reflectivity can range from four percent down to less than one hundredth of one percent (with anti-reflective coatings). For amplifiers with beveled ends (angled windows) the reflectivity can be set to zero.

Length The amplifier length is limited by the available memory and the patience of the user. Longer amplifiers require smaller step sizes, longer run times and, depending on the time step used, can cause data storage problems.

Diameter There are no model limits on the diameter of the amplifier, however, the user should keep in mind that the smaller the diameter for a given input amplitude, the higher the intensity. High intensities require smaller time steps to keep the relative error within reasonable limits. So, smaller diameters can lead to problems similar to those encountered with long length inputs.

Oscillator Volume/Input Amplitude These inputs also determine the intensity of the input pulse. For the "filed-pulse" routine, the oscillator volume parameter is used in

the conversion from megawatts per liter to photons per cubic meter. A typical value is one liter. For the square-pulse routine, the value for input amplitude is limited only by the resulting intensity. The input screen displays and updates the intensity for changes in diameter as well as input amplitude. Smaller input amplitudes and/or larger diameters are recommended to keep the intensity under 10 MW/cm^2.

Kinetics The user has an option to allow the population inversion to be developed by gas kinetics or to "turn off" the gas kinetics and let only the incoming pulse affect the inversion. If the kinetics are turned off, the user must input a value for the initial gain coefficient. Typical values range from 50 to 200 percent per meter.

Amplified Spontaneous Emissions For CO_2 amplifiers less than two meters long, ASE is not a significant loss factor unless the gain is over 300 percent per meter. However, as amplifiers get longer, ASE becomes an important factor at lower values of gain. For example, ASE can reach saturation intensity in a six meter amplifier with a gain of only 120 percent per meter.

A.2 Filed-Pulse Routine

The filed-pulse routine begins during the output portion of Stone's oscillator model. Here, files are created to store parameter input data and power output data. Files must be created using a "file step" of one. That is, each data point should be saved. This is because the amplifier uses one time step at a time and must have an input value for each time step.

Most oscillator runs use two time steps. With this "change-time-step" option, the first time step (h1) is for the pulse portion of the output and the second, larger time step (h2) is for the linear portion of the output. The amplifier model can only use one time step because the time step defines the number of amplifier divisions. Data saved using the "change-time-step" option can be used as an input to the amplifier model only if the value for h2 is divisible by h1. In this way, h1 will be the amplifier's time step and extra input values will be calculated by simple linear interpolation. For example, if h1 is 0.1 and h2 is 2.0 then 20 input values have to be calculated between each h2 increment.

Ideally, the time step used in the oscillator will be small enough to provide accurate amplifier results. If not, the user can cut his time step in half. Again, linear interpolation will be used to calculate the additional input values. The time step can be cut in half as many times as memory will permit.

A.3 Square-Pulse Routine

With respect to time steps, the square-pulse routine is more flexible than the filed-pulse routine. The user can choose any time step or number of cell divisions without consideration for a file of input values. Though this routine allows only square input pulses, the user is in control of pulse amplitude and pulse duration.

When adjusting the start and stop times for the square input pulse, the user will see on the screen display that the total run time also changes. As an explanation for this change consider an amplifier divided into five cells. Each cell has a length of one time step. If the pulse starts at the first time step and ends on the tenth, it takes a total of fifteen time steps for the entire pulse to exit the amplifier. To allow the pulse to completely pass through the amplifier, the total run time must extend at least five time units past the stop time of the pulse.

Another facet of the square-pulse routine is a comparison between the model's energy gain and the energy gain derived using Frantz and Nodvik's closed form solution. Originally, this comparison was used for validation purposes, but it has been left in the model to give the user a feel for the model's accuracy. To see this comparison, the user must set up the following conditions:

1. Turn off kinetics.
2. Set reflectivity to zero.
3. Set ASE value to "n."

A.4 Screen Displays

While the program is running, the screen will display the elapsed time in seconds, the amount of work completed in percent, and the current time step. A second row of

data displays updated values for the ASE output, the pulse output, and the gain in a predetermined cell. The user will be given an option as to which cell is to be monitored. At the completion of the run, another set of numbers will be listed on the screen. This set of numbers represents the gain in each cell across the amplifier.

Following the completion of the run the user has a choice of two output data displays. The first display shows the time variation of gas populations (N_2, $CO_2(001)$, and $CO_2(100)$) along with the power input (Pin), the power output (Pout), and the gain in a predetermined amplifier cell (Gain#). The second display trades the gas populations for columns showing the time variation of the energy output, the ASE output, and the gain in the first amplifier cell.

The displays are basically self-explanatory. However, one point that should be made clear deals with the lag time between a pulse input unit and its corresponding output. To compare an input unit to its output, the screen display should be displayed with an increment of one. Then to locate the output for an specific input, the user must count down a number of time steps equal to the number of amplifier divisions.[2] Understanding this time lag makes it easier to see how a pulse's shape is altered after passing through an amplifier.

A.5 Storing Files

Once the run is complete, the user has three options. He can skip between the output screens at will, he can start over, or he can choose to make data files for future use. Data files can be made for the following outputs: populations, energy, ASE, gain, and power. For each data file created, a supplemental file is also created. This file contains various information about the particular amplifier run.

Data is stored in a simple format. Each line of data begins with its time reference and is followed by the data element. The files have suffixes that let the user know which data set is in which file. All of the data files have one data element except for the power data file. It has elements for both the input and output power.

[2] Each amplifier division corresponds to one time unit.

A.6 Overcoming Memory Limitations

Modeling long amplifiers not only requires smaller time steps and very long run times, it can also cause data storage problems. Personal computers have limitations on the amount of random access memory available for applications programs. In our program, storage of output array data consumes the most memory. The sizes of these arrays depend on amplifier length, time step, and maximum run time. Maximum run time is important because data is stored for each time step. Depending on the gas kinetics, the amplifier might require a relatively long period of time to establish its high gain profile. In such a case, memory might be insufficient to even begin the run.

To overcome this limitation, the model can be used to generate the output data for the amplifier one section at a time. For example, a fifteen-meter amplifier might be modeled as three consecutive five-meter amplifiers or five consecutive three-meter amplifiers. The only designs where this technique is applicable are those amplifiers with anti-reflective coatings on its windows. There are two reasons for this limitation. First, ASE calculations would be completely unreasonable. Second, there would be additional window losses because each section would add two more windows to the overall model. We use only one input parameter to describe the reflectivity of both amplifier windows. So, even if we set the reflectivity to zero for all but the first and last section, we will still have two extra window losses.

The first test accomplished was to compare the output of an entire fifteen-meter amplifier to one that had been cut into three sections. Using zero reflectivity and identical time steps, the outputs agreed to six decimal places. Next, we divided the whole amplifier into 20 cells and the amplifier made of sections into 60 cells (20 cells per section). Figure A.1 compares the outputs for these two cases. Curve A represents the 20 cell amplifiers output. Curve B is sharper because its leading edge experiences slightly higher gain. As mentioned earlier, increasing the number of cells allows the kinetics to go through more iterations and develop higher gain at the end of the amplifier. Higher gain allows more energy to be extracted sooner, so curve B falls off faster than curve A. This more refined pulse shape shows the advantage of using a series of short amplifiers to model one very long one.

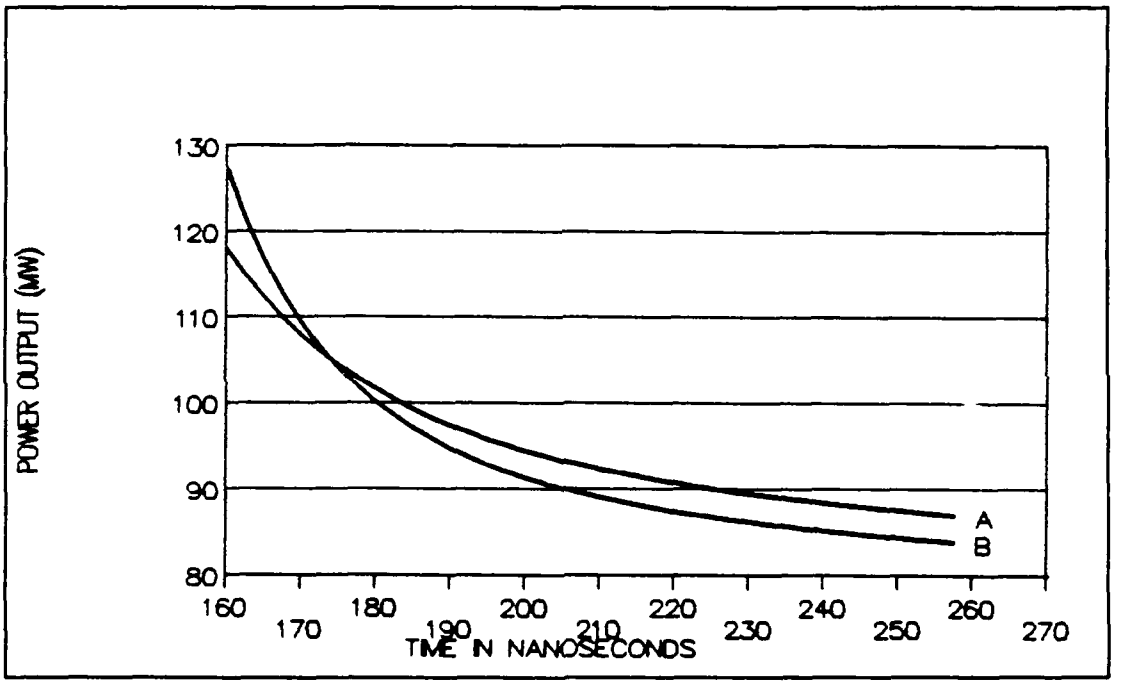

Figure A.1. Output pulse calculated using (A) 20 cells and (B) 60 cells

Appendix B. *Derivation of Factor1*

The output from Stone's oscillator model has units of megawatts per liter of oscillator volume. For consistency, the input file generated during the square pulse routine also has these units. This amplifier uses photons per cubic meter as its base unit. To get from megawatts/liter to photons/meter^3, the first step is to multiply by the oscillator volume to arrive at megawatts. Then Factor1 is used to complete the conversion. Factor1 considers the time step used (tcav × h1), the cross-sectional area of the amplifier (*Area*), and the frequency of the output beam (ν).

The time step determines the energy contained in each power unit and how much linear distance the power unit will occupy in the amplifier: x = c × tcav × h1. The cross-sectional area completes the calculation for the volume filled by the photons of the power unit. The frequency determines the energy per photon by the expression $E = h\nu$, where h is Planck's constant.

Step by step, Factor1 is given by the following:

- Megawatts to watts ⟶ (MW) ×(1000000)
- Watts to Photons/second ⟶ (W) ÷($h\nu$)
- Photons/second to photons ⟶ (photons/second) × (tcav × h1)
- Photons to photons/m^3 ⟶ (photons) ÷ (Area × c × tcav × h1)

When simplified the equation for Factor1 is:

$$Factor1 = \frac{1000000}{(h\nu)(\mathrm{c})(\mathrm{Area})} \tag{B.1}$$

Appendix C. *ASE Analytic Solution*

In this appendix, we will summarize our analysis into the reason why our results for ASE gain limits were consistently higher than those calculated with a basic analytical equation.

C.1 Basic Equation

Both Milonni and Verdeyen described the condition where ASE reaches saturation intensity (14, 24:400,183). Their derivations are different, but they arrive at similar results for an expression for the maximum permissible gain in an amplifier. Milonni and Verdeyen begin with the equation for radiation traveling in the positive **z** direction:

$$I(z) = \left(\frac{A_{21} h\nu \Omega}{4\pi}\right)\left(\frac{N_2}{g}\right)(e^{gz} - 1) \tag{C.1}$$

where N_2 is the population of the upper level and g is the gain coefficient. By allowing $I(z)$ to be the saturation intensity for the amplifier, they arrive at an intermediate solution:

$$e^{gL} - 1 < \frac{1/A_{21}}{\tau_2}\frac{4\pi}{\Omega}\left(\frac{N_2 - N_1}{N_2}\right). \tag{C.2}$$

Following the three assumptions described below, they arrive at

$$e^{gL} - 1 < \frac{16L^2}{d^2} \tag{C.3}$$

as the equation limiting the amplifier's gain, length, and diameter. When the left-hand side of this equation becomes greater than the right-hand side, ASE will significantly affect the operation of the amplifier.

C.2 Analysis of Assumptions

The three assumptions used to arrive at this simple equation are not used in our model. Therefore, we examined these assumptions to determine the reason our amplifier

model required significantly higher values for g to cause ASE to reach saturation intensity. The three assumptions are:

1. $\dfrac{N_2}{(N_2 - N_1)} = 1.$
2. $\Omega = \dfrac{Area}{L^2} \longrightarrow \dfrac{16L^2}{d^2}.$
3. $\dfrac{1/A_{21}}{\tau_2} = 1.$

Using typical values for the populations of the upper and lower laser levels we found that as the gain increased, the validity of the first assumption also increased. Table C.1 shows this trend. Because this assumption is valid for high values for the gain coefficient,

Table C.1. Relationship between gain coefficient and the ratio $N_2/(N_2 - N_1)$

g (%/m)	Ratio
5	2.92
10	1.96
20	1.48
40	1.24
80	1.12
160	1.06

it does not explain the difference between the model's results and the analytic equation.

Next, we looked at the approximation for solid angle, $Area/L^2$. While this value is adequate for positions close to the beginning of the amplifier, it underestimates all values closer to the end. Table C.2 shows how the solid angle varies for positions in an amplifier and indicates the magnitude of the error by tabulating values for [Integral Solution/Approximation]. (The positions are based on a one-meter amplifier.) Equation C.3 shows that gain is limited by the reciprocal of the solid angle. Thus, these large differences between the actual and the approximate values for solid angle indicate that the actual value for the gain limit is higher than that given by Equation C.3.

This is only a partial explanation for our model's results. Though the solid angles are larger, the actual contribution to ASE output is still rather small for positions near the

Table C.2. Comparison between solid angle approximation and an integral solution

Position (m)	Appoximation	Integral	$\frac{Integral}{Approx.}$
0.0	0.00196	0.00196	1.00
0.1	0.00196	0.00242	1.23
0.2	0.00196	0.00306	1.56
0.3	0.00196	0.00400	2.03
0.4	0.00196	0.00544	2.77
0.5	0.00196	0.00784	3.99
0.6	0.00196	0.01224	6.23
0.7	0.00196	0.02170	11.1
0.8	0.00196	0.04852	24.7
0.9	0.00196	0.18760	95.5

end of the amplifier. Photons emitted at these positions are amplified over only a short distance, so their ability to extract energy is very limited.

The best explanation for our model's results was found upon examining the last assumption. In CO_2 lasers, the lifetime of the upper vibrational level depends not only on its slow spontaneous emission rate, but also on a high rate of collisional relaxation. Therefore, the lifetime of the upper state, (τ_2), is far shorter than $1/A_{21}$. This makes the value for $\frac{1/A_{21}}{\tau_2}$ much greater than one and explains why our value for the gain allowing ASE to reach saturation intensity is higher than the gain calculated with Equation C.3.

Appendix D. *ASE Variations Due to Large Solid Angles*

In addition to causing timing errors for input pulse reflections, fractional cells also played a role in causing asymmetric ASE outputs. In our model, the fractional cell is always the last cell. Because of this, the solid angle subtended in the positive direction at the final cell is always greater than the solid angle subtended in the negative direction at the first cell. Therefore, if a fractional cell exists, the ASE outputs will never be perfectly symmetric.

Until the gain in the fractional cell is depleted, the ASE output from the positive end of the amplifier will have a larger value. ASE is a function of A_{21}, population of the upper vibrational level, cell length, and solid angle. To compare the outputs at the two ends, we need only consider the last two. For example, if we have a cell length of 30 centimeters and a diameter of 5 centimeters, our model calculates $\Omega/4\pi$ to be 0.0068. If the fractional cell is only two centimeters long, its value for $\Omega/4\pi$ is .3143. Including the length difference, the amount of ASE that leaves the last cell is triple the amount that leaves the first cell. While this causes a loss in symmetry, it actually makes our approximate ASE output value closer to the theoretical value.

In general, the shorter the cells are, the higher the value for ASE output will be. This is true with or without fractional cells. The large values for $\Omega/4\pi$ occur only when measured at distances within a diameter's length from the end of the cavity and the maximum value for $\Omega/4\pi$ is only 0.5. So, for the last few centimeters of the amplifier, our model underestimates the ASE output. The amount of the error increases for longer cell lengths. For cell lengths smaller than 30 centimenters (time steps $<$ one nanosecond) the error is insignificant when compared to the ASE output for the entire amplifier. Additionally, because of our line shape approximation, we still have a conservative approximation for the ASE output.

Bibliography

1. Allen, L. and G. I. Peters. "Amplified Spontaneous Emission and External Signal Amplification in an Inverted Medium," *Physical Review A*, 8: 2031-2046 (October 1973).
2. Chow, Weng W. "Amplified Spontaneous Emission Effects in Laser Amplifiers," *SPIE Proceedings*, 1045: 139-147 (1989).
3. Comly, J. C. Jr. *et al.* "Discharge and Kinetics Modeling in Electron-Beam Controlled CO_2 Laser Amplifiers," *IEEE Journal of Quantum Electronics*, QE-17: 1786-1798 (September 1981).
4. Douglas-Hamilton, D. H. *et al. Carbon Dioxide Electric Discharge Laser Kinetics Handbook.* Technical Report AFWL-TR-74-216. AVCO Everett Research Laboratories, Everett MA, June 1974 (AD-A008 650).
5. Frantz, Lee M. and John S. Nodvik. "Theory of Pulse Propagation in a Laser Amplifier," *Journal of Applied Physics*, 34: 2346-2349 (1963).
6. Frey, R. W. *et al.* "Laser Imaging Radar Sensor (LIRS)," *SPIE Proceedings*, 500: 2-9 (1984).
7. Gilbert, J. *et al.* "Dynamics of the CO_2 Atmospheric Pressure Laser with Transverse Pulse Excitation," *Canadian Journal of Physics*, 50: 2523-2535 (October 1972).
8. Glazenkov, V. M. *et al.* "Experimental Determination of the Parameters of Vibrational-Rotational Transitions in Isotopic Forms of CO_2 Molecules," *Soviet Journal of Quantum Electronics*, 18: 534-536 (April 1988).
9. Harney, R. C. "Comparison of Techniques for Long-Range Laser Ranging," *SPIE Proceedings*, 783: 91-100 (1987).
10. Harney, R. C. "Military Applications of Coherent Infrared Radar," *SPIE Proceedings*, 300: 2-11 (1981).
11. Manes, K. R. and H. J. Seguin. "Analysis of the CO_2TEA Laser," *Journal of Applied Physics*, 43: 5073-5078 (December 1972).
12. McQuillan, A. K. and A. I. Carswell. "Spatially Resolved Gain Measurements in a CO_2 Amplifier," *Canadian Journal of Physics*, 50: 769-777 (1972).
13. Melançon, T. B. *A Model of Temperature Effects in Pulsed and Continuous Wave CO_2 Laser Models and Optimization Using Response Surface Methodology.* MS Thesis (work in progress), AFIT/GSO-89D. School of Engineering, Air Force Institute of Technology, Wright-Patterson AFB, Ohio, December 1989.
14. Milonni, Peter W. and Joseph H. Eberly. *Lasers.* New York: John Wiley and Sons, 1988.
15. Pace, Paul, *et al.* "Frequency-Stabilized Transversely Excited Atmospheric (TEA) CO_2 Lasers for Coherent Infrared Radar Systems," *SPIE Proceedings*, 300: 148-152 (1981).

16. Patel, C. K. N. "CO_2 Lasers," *Scientific American*: 23-34 (August, 1968).

17. Pressley, Robert J. *CRC Handbook of Lasers.* Cleveland, OH: The Chemical Rubber Company, 1971.

18. Reilly, James P. "CO_2 Frequency Stable Amplifier Assessment," *SPIE Proceedings*, 783: 60-68 (1987).

19. Rooth, R. A., J. A. van der Pol, and E. H. Hasselhoff. "Intramode and Fermi Relaxation in CO_2, Their Influence on Multiple-Pass, Short-Pulse Energy Extraction," *Applied Physics B*, 42: 103-110 (September 1986).

20. Schulz-Dubois, E. O. "Pulse Sharpening and Gain Saturation in Traveling-Wave Masers," *Bell Systems Technical Journal*, 3: 625-658 (March 1964).

21. Slater, Philip N. *Remote Sensing.* Reading, MA: Addison-Wesley Publishing, 1980.

22. Stone, David H. Class lecture for Physics 520, Introduction to Laser Physics. School of Engineering, Air Force Institute of Technology (AU), Wright-Patterson AFB OH, Fall 1988.

23. Tsunawaki, Y. "Copper and Molybdenum Mirrors for High Power TEA CO_2 Lasers," *SPIE Proceedings*, 1019: 414-415 (1988).

24. Verdeyen, Joseph. *Laser Electronics.* Englewood Cliffs, NJ: Prentice-Hall, 1981.

25. Witteman, W. J. *The CO_2 Laser.* Heidlberg, Germany: Springer-Verlag Berlin, 1987.

26. Yoder, M. J. *et al.* "Development of CO_2 Laser Amplifiers for Radar Applications," *SPIE Proceedings*, 709: 46-51 (1986).

Vita

Frank Patrick Gallagher II [redacted] He [redacted] in 1980 [redacted] moved to Colorado Springs, Colorado to attend the United States Air Force Academy. In 1985, he received the degree of Bachelor of Science in Civil Engineering. After graduation, he entered active duty in the Air Force and served as an Orbital Analysis Officer in the Space Surveillance Center at Cheyenne Mountain Air Force Base. In May of 1988, he entered the School of Engineering, Air Force Institute of Technology at Wright Patterson Air Force Base, Ohio.

[redacted]

REPORT DOCUMENTATION PAGE

Form Approved
OMB No. 0704-0188

1a. REPORT SECURITY CLASSIFICATION: UNCLASSIFIED	1b. RESTRICTIVE MARKINGS
2a. SECURITY CLASSIFICATION AUTHORITY	3. DISTRIBUTION / AVAILABILITY OF REPORT: Approved for public release; distribution unlimited
2b. DECLASSIFICATION / DOWNGRADING SCHEDULE	
4. PERFORMING ORGANIZATION REPORT NUMBER(S): AFIT/GSO/ENP/ENS/89D-2	5. MONITORING ORGANIZATION REPORT NUMBER(S)
6a. NAME OF PERFORMING ORGANIZATION: School of Engineering; 6b. OFFICE SYMBOL (If applicable): AFIT/ENP/ENS	7a. NAME OF MONITORING ORGANIZATION
6c. ADDRESS (City, State, and ZIP Code): Air Force Institute of Technology, Wright-Patterson AFB, OH 45433-6583	7b. ADDRESS (City, State, and ZIP Code)
8a. NAME OF FUNDING / SPONSORING ORGANIZATION: WRDC; 8b. OFFICE SYMBOL (If applicable): AARI	9. PROCUREMENT INSTRUMENT IDENTIFICATION NUMBER
8c. ADDRESS (City, State, and ZIP Code): Wright-Patterson AFB, OH 45433	10. SOURCE OF FUNDING NUMBERS: PROGRAM ELEMENT NO. / PROJECT NO. / TASK NO / WORK UNIT ACCESSION NO.

11. TITLE (Include Security Classification)

NUMERIC MODEL OF A CO_2 LASER AMPLIFIER (UNCLASSIFIED)

12. PERSONAL AUTHOR(S)
Frank P. Gallagher, B.S., Captain, USAF

13a. TYPE OF REPORT	13b. TIME COVERED	14. DATE OF REPORT (Year, Month, Day)	15. PAGE COUNT
MS Thesis	FROM _____ TO _____	1989 DECEMBER	80

16. SUPPLEMENTARY NOTATION

17. COSATI CODES			18. SUBJECT TERMS (Continue on reverse if necessary and identify by block number)
FIELD	GROUP	SUB-GROUP	Carbon Dioxide; Laser; Amplifier; Model; Amplified Spontaneous Emission
09	03		

19. ABSTRACT (Continue on reverse if necessary and identify by block number)

Thesis Advisor: Dr. David H. Stone
Assistant Professor
Department of Engineering Physics

20. DISTRIBUTION / AVAILABILITY OF ABSTRACT: ☒ UNCLASSIFIED/UNLIMITED ☐ SAME AS RPT. ☐ DTIC USERS	21. ABSTRACT SECURITY CLASSIFICATION: UNCLASSIFIED
22a. NAME OF RESPONSIBLE INDIVIDUAL: David H. Stone, Assistant Professor	22b. TELEPHONE (Include Area Code): (513) 255-4498; 22c. OFFICE SYMBOL: ENP

DD Form 1473, JUN 86 *Previous editions are obsolete.*

Abstract

A CO_2 laser amplifier simulation model is developed for use on IBM-compatible personal computers. First, a general laser amplifier is modeled by dividing an amplifier into separate cells to model both the temporal and spatial dependence of the amplifier's gain. The resulting amplification is validated by comparison with a closed-form solution. Second, losses due to amplified spontaneous emissions (ASE) are investigated and included in the model. Equations for ASE losses consider both the solid angle of the emissions and the reflectivity of the cavity windows. Other reflections are ignored. Third, an existing numerical model of CO_2 gas kinetics is incorporated. In this kinetics model, temperature-dependent terms are fixed according to initial conditions, and the rotational levels of the upper CO_2 vibrational state are assumed to be in equilibrium.

The user-friendly model allows designers and students to investigate the amplification of either square input pulses or pulses generated with a laser oscilltor while varying several input parameters. Among the variable parameters are length, diameter, gas mix, temperature, pressure, window reflectivity, and pump efficiency.